Published in final edited form as:
Dev Biol. 2010 August 15; 344(2): 809–826. doi:10.1016/j.ydbio.2010.05.513.

Nrk2b-mediated NAD+ production regulates cell adhesion and is required for muscle morphogenesis *in vivo*

Michelle F. Goody[1], **Meghan W. Kelly**[1], **Kevin N. Lessard**[1], **Andre Khalil**[2,3,4], and **Clarissa A. Henry**[1,2,4]

[1]School of Biology and Ecology, University of Maine, Orono, ME 04469 USA

[2]Institute for Molecular Biophysics, The Jackson Laboratory, Bar Harbor, ME 04619 USA

[3]Department of Mathematics and Statistics, University of Maine, Orono, ME 04469 USA

[4]Graduate School of Biomedical Sciences, University of Maine, Orono, ME 04469 USA

Abstract

Cell-matrix adhesion complexes (CMACs) play fundamental roles during morphogenesis. Given the ubiquitous nature of CMACs and their roles in many cellular processes, one question is how specificity of CMAC function is modulated. The clearly defined cell behaviors that generate segmentally reiterated axial skeletal muscle during zebrafish development comprise an ideal system with which to investigate CMAC function during morphogenesis. We found that Nicotinamide riboside kinase 2b (Nrk2b) cell autonomously modulates the molecular composition of CMACs *in vivo*. Nrk2b is required for normal Laminin polymerization at the myotendinous junction (MTJ). In Nrk2b-deficient embryos, at MTJ loci where Laminin is not properly polymerized, muscle fibers elongate into adjacent myotomes and are abnormally long. In yeast and human cells, Nrk2 phosphorylates Nicotinamide Riboside and generates NAD+ through an alternative salvage pathway. Exogenous NAD+ treatment rescues MTJ development in Nrk2b-deficient embryos, but not in *laminin* mutant embryos. Both Nrk2b and Laminin are required for localization of Paxillin, but not β-Dystroglycan, to CMACs at the MTJ. Overexpression of Paxillin in Nrk2b-deficient embryos is sufficient to rescue MTJ integrity. Taken together, these data show that Nrk2b plays a specific role in modulating subcellular localization of discrete CMAC components that in turn play roles in musculoskeletal development. Furthermore, these data suggest that Nrk2b-mediated synthesis of NAD+ is functionally upstream of Laminin adhesion and Paxillin subcellular localization during MTJ development. These results indicate a previously unrecognized complexity to CMAC assembly *in vivo* and also elucidate a novel role for NAD+ during morphogenesis.

Keywords

skeletal muscle; cell-matrix adhesion; nicotinamide riboside kinase; nicotinamide adenine dinucleotide; laminin; paxillin

Author for correspondence: Clarissa Henry, School of Biology and Ecology, 5735 Hitchner Hall Room 217, University of Maine, Orono, ME, 04469-5735, Clarissa.Henry@umit.maine.edu, Phone (207) 581-2816, Fax (207) 581-2537.

Introduction

One fundamental question in developmental biology is how tissue architecture is generated and maintained. Both cell-cell adhesion and cell-matrix adhesion are critical for organogenesis. However, despite the spatial and temporal regulation of cell adhesion in nearly all morphogenetic events, the dynamic modulation of cell adhesion during morphogenesis is not well understood. Zebrafish axial skeletal muscle, because of its reiterated nature and simple structure, is an ideal model system with which to analyze the molecular details of cell adhesion complex assembly and specificity of cell adhesion dynamics during different cellular behaviors.

Cell-matrix adhesion mechanically links cells to the extracellular matrix (ECM) through transmembrane receptors (e.g. Integrins). *In vitro*, these adhesion sites have different names depending on their size and composition (Geiger et al., 2001). A recent review proposed use of the umbrella term Cell-Matrix Adhesion Complexes (CMACs, pronounced *seeMACs*) to refer to all cell-matrix adhesion structures (Lock et al., 2008). CMACs are dynamic structures that are alternately formed and disassembled during cell migration. CMAC assembly involves Integrin clustering and the recruitment and phosphorylation of numerous cytoplasmic proteins that link to the cytoskeleton. Two well known cytoplasmic proteins that modulate dynamic adhesion are Focal Adhesion Kinase (FAK) and Paxillin. FAK is a non-receptor tyrosine kinase that is phosphorylated upon adhesion to the ECM (Schaller et al., 1992). FAK is overexpressed in many types of cancerous cells (Chatzizacharias et al., 2008) and is thought to promote cell motility by facilitating CMAC turnover (Ilic et al., 1995). Counter intuitively, FAK also plays a role in stabilizing adhesion: FAK is required for costamerogenesis in muscle cells (Quach and Rando, 2006) and FAK concentration increases subsequent to muscle loading (Gordon et al., 2001). Similarly, the scaffolding protein Paxillin can also promote both CMAC assembly and disassembly. Paxillin is one of the first proteins recruited to nascent CMACs and is hypothesized to play a role in mediating the molecular composition of assembling CMACs (Digman et al., 2008). However, Paxillin is also required for adhesion turnover: cells without Paxillin exhibit stabilized adhesions (Webb et al., 2004). Many *in vitro* studies have looked at the order in which intracellular proteins are recruited to CMACs. The uniting conclusion from these studies is that the order of recruitment is context dependent. Even less is known about CMAC dynamics *in vivo*. Given the complexity of CMACs *in vitro*, along with the fact that the same proteins can promote different cellular behaviors, it is likely that a complex combinatorial code of the post-translational modifications and interactions of CMAC proteins mediates cell behavior *in vivo*.

One important question is how an adhesion code mediates interaction of cells with their ECM microenvironment. The bi-directional signaling that occurs between cells and their ECM through CMACs is called “dynamic reciprocity” (Bissell et al., 1982). Signaling from the ECM modifies intracellular signaling, gene expression and cell morphology. Signals from within the cell modify the molecular composition and structure of the ECM. The basement membrane is one specialized compartment of the ECM and is required for muscle development and physiology. Basement membranes surround individual muscle fibers and concentrate at the myotendinous junction (MTJ). Adhesion to Laminin in basement membranes is critical for muscle development in both zebrafish and mice (Guyon et al., 2007; Kanagawa and Toda, 2006; Lieschke and Currie, 2007; Schessl et al., 2006). Multiple human myopathies result from disruption of muscle to basement membrane adhesion (Kanagawa and Toda, 2006; Schessl et al., 2006). Despite the critical importance of adhesion between muscle and the basement membrane, the mechanisms that mediate initial attachment and assembly/polymerization of the basement membrane are not known.

Given the ubiquitous and dynamic nature of cell adhesion, one fundamental question is how cell adhesion modulates multiple different cell behaviors. Muscle Integrin Binding Protein (MIBP) is a novel, muscle-specific protein that binds to the Laminin receptor Integrin α7β1 (Li et al., 1999). MIBP is a splice variant of Nicotinamide riboside kinase 2 (Nrk2), which has also been designated Integrin β1 Binding Protein 3 (ITGβ1BP3). Human Nrk1 and Nrk2 phosphorylate Nicotinamide Riboside to generate Nicotinamide Adenine Dinucleotide (Belenky et al., 2007b; Bieganowski and Brenner, 2004; Tempel et al., 2007). Several lines of evidence suggest that Nrk2 plays a critical role in muscle development and physiology: (1) overexpression of *mibp* disrupts myotube formation *in vitro* (Li et al., 2003), (2) *itgβ1bp3* is the second most upregulated muscle transcript in *myostatin* −/− cows (Sadkowski et al., 2008), and (3) *nrk2* is the most highly upregulated tissue restricted transcript in alveolar soft-part sarcoma (Stockwin et al., 2009). Taken together, these data suggest that Nrk2 is a critical regulator of muscle growth and development. Thus, we asked whether Nrk2 is required for animal development in general and zebrafish muscle development specifically.

There are at least two zebrafish orthologues of Nrk2. We focused on Nrk2b (a.k.a. MIBP2) because it is expressed during muscle development. We used morpholino-mediated knockdown to ask whether Nrk2b is required for muscle development *in vivo*. Embryos injected with morpholinos targeted to *nrk2b* resemble *laminin* mutants, suggesting that *nrk2b* functions to mediate adhesion to Laminin *in vivo*. In support of this, *laminin γ1* mutants injected with *nrk2b* morpholinos resemble *laminin γ1* mutants injected with control morpholinos. This epistasis analysis suggests that *nrk2b* functions in the Laminin signaling pathway. Although a basement membrane at the MTJ does form in *nrk2b* morphants, it is significantly less organized than in control embryos. Genetic mosaic analysis suggests that Nrk2b is non-cell autonomously required for proper basement membrane polymerization. However, Nrk2b is cell autonomously sufficient for localization of Paxillin to CMACs at the MTJ. To our knowledge, this is the first identification of a vertebrate protein that cell autonomously mediates the molecular complexity of CMACs *in vivo*. Human and yeast Nrk proteins function in an alternative salvage pathway to generate NAD+ (Belenky et al., 2007a; Belenky et al., 2009; Belenky et al., 2007b; Bieganowski and Brenner, 2004; Bogan and Brenner, 2008). Exogenous NAD+ rescues discontinuous MTJs in *nrk2b* morphants but not in *laminin γ1* mutants. These data suggest that Nrk2b-mediated NAD+ production functions upstream of Laminin adhesion/signaling during zebrafish muscle morphogenesis. Taken together, these data show that this understudied protein and NAD+ are novel cell adhesion regulators that impart specificity to the assembly of cell adhesion complexes.

Materials and Methods

Zebrafish (Danio rerio) husbandry/Mutant lines/Transgenic lines

Adult zebrafish were kept at 28.5°C on a 16 hour light/8 hour dark cycle. Zebrafish embryos were collected from natural spawnings of these adult fish. Embryos were staged according to Kimmel et al., 1995. *Gup/laminin β1*^{tg210} and *sly/laminin γ1*^{ti263A} mutants were a generous gift from the Tuebingen stock center. A transgenic line expressing GFP fused to the C-terminus of Paxillin was generated by cloning full length Paxillin off 24 hours post fertilization (hpf) zebrafish cDNA, cloning the PCR product into the pDONR221 plasmid (Invitrogen) and then cloning, along with p5E-*bactin2* (ubiquitous beta-actin promoter, a 5' entry clone vector from the Tol2Kit (Kwan et al., 2007)) and p3E-EGFPpA (EGFP for C-terminal fusions, plus SV40 late polyA, a 3' entry clone vector from the Tol2Kit (Kwan et al., 2007)), into a pDestTol2pA plasmid (a destination vector from the Tol2Kit (Kwan et al., 2007)) via a recombination reaction. Linearized pCS2-TP plasmid (kindly provided by Koichi Kawakami) was used as a template to generate capped mRNA encoding Tol2 transposase by *in vitro* transcription using SP6 polymerase (Message Machine, Ambion).

Plasmids were co-injected with mRNA encoding Tol2 transposase into embryos at the single cell stage. GFP expressing zebrafish from the F_0 generation were grown up and then spawned to detect for germ line incorporation of the transgene. The F_1 generation, offspring of the F_0 generation with germ line incorporation of the transgene, stably overexpressing Paxillin was used for experimentation.

Morpholino (MO) injections

MOs were obtained from Gene Tools, LLC. The nucleotide sequence of the *nrk2bm1* MO is 5'-GAACTTCATCCTCGACGTGATTTT G-3' and the sequence of the *nrk2bm2* MO is 5'-CGTCAAAGTAGAGAAAAATTGG CTA-3'. The sequence of the standard control MO is 5'-CCTCTTACCTCAGTTACAATTTATA-3'. All MOs were diluted in sterile water. The *nrk2b* MO cocktail was 12 ng *nrk2bm1* plus 6 ng *nrk2bm2*. 12 ng of the standard control MO was injected. *dystroglycan* MO was injected according to Parsons et al., 2002. The *p53* MO sequence is 5' -CCCTTGCGAACTTACATCAAATTCT - 3'. Equal amounts of *nrk2b* MOs and the *p53* MO were combined and co-injected. MOs were injected with a MPPI-2 Pressure Injector from ASI. Embryos were injected in the yolk at the 1-cell stage. The *laminin* MOs used have been previously described and recapitulate the mutant phenotype (Parsons et al., 2002b).

Suppression of GFP fluorescence when the target sequence is co-injected with MOs: Full length *nrk2b* was amplified off cDNA from 24 hpf zebrafish. The PCR product was cloned using the Tol2Kit and injected as above, with or without *nrk2b* MOs.

NAD+ treatment

β-NAD (Sigma) was dissolved in Embryo Rearing Medium to a stock concentration of 15 mM. The treatments used were 100 μM and 1 mM NAD+ (Jones et al., 2008). Embryos were treated from shield stage through live imaging/fixation.

Antibody (Ab) staining/immunohistochemistry

All Abs were diluted in block (5% w/v Bovine Serum Albumin (BSA) in Phosphate Buffered Saline (PBS) with 0.1% Tween20). Alexa Fluor 488 phalloidin (Molecular Probes) staining involved fixing embryos in 4% Paraformaldehyde (PFA) for 4 hours at room temperature (RT), washing 5 times for 5 minutes each (5×5) in 0.1% PBS-Tween, permeabilizing for 1.5 h in 2% PBS-Triton, washing 5×5 and then incubating in phalloidin (1:20) for 1–4 hours at RT. Ab staining followed phalloidin staining or started with blocking for 1 hour at RT, incubating in 1° Ab overnight at 4°C, washing for 2–8 hours at RT, incubating in 2° Ab overnight at 4°C, then washing for 1 hour. 1° Abs: anti-β-Catenin 1:500 (Sigma); anti-β-Dystroglycan 1:50 (Novocastra); anti-Laminin-111 1:50 (Sigma); anti-Paxillin 1:50 (BD Biosciences); anti-pan-FAK-c-20 1:50 (Santa Cruz Biotechnology); anti-pY-397-FAK, anti-pY-861-FAK 1:50 (Biosource). 2° Abs: GAM/GAR 488, 546, 633 1:200 (Invitrogen).

Whole mount in situ hybridization (ISH)

Dechorionated embryos were fixed and washed as above, treated with Proteinase K (Fisher) for 1 to 15 minutes and then fixed (20 minutes) and washed 5×5. Embryos were incubated in prehybridization solution (50% Formamide, 5× sodium chloride-sodium citrate buffer, 50 μg/mL Heparin, 500 μg/mL Yeast tRNA, 0.1% Tween20, pH of 6.0 with citric acid) for 4 hours at 65°C, and then hybridized overnight at 65°C with a digoxygenin-labeled probe. Embryos were washed in PBS-Tween, incubated in anti-digoxygenin Ab (Roche) for 2 hours at RT, washed and then developed in a 0.45% NBT/0.35% BCIP (Roche) in PBS-Tween solution until the desired color was obtained. Controls and morphants hybridized

with the same probe were developed for the same amount of time. The developing process was stopped by fixing or rinsing 4 times in sterile water.

Westerns

Protein was prepared from 24 hours post fertilization zebrafish embryos using previously described methods (Link et al., 2006). Protein was resolved on a 10% SDS-PAGE gel, transferred to PVDF membrane, blocked in 5% dry milk, incubated in 1° Ab (anti-Paxillin 1:1000, BD Biosciences) at 4°C overnight, washed, incubated in 2° Ab, washed, detected with Supersignal West Dura (Pierce) and developed on a CCD LAS 4000 Fuji camera.

Genetic mosaics

Embryos were injected with MOs as described above and 10,000 MW fluorescent (wavelength 546 or 633) dextrans (Molecular Probes). Transplants were performed as described in Henry and Amacher, 2004.

Comparative qRT-PCR

RNA was isolated from whole embryos at 24 hpf via Qiagen's RNeasy Mini Kit. One-step comparative qRT-PCR was conducted with Quanta kit reagents and Rox reference dye. A Mx400 machine was used and the annealing temperature was 60°C. Approximately 50 ng of RNA template was used per reaction. We used *β-actin* as our normalizing transcript. See Supplementary Table 1 for a complete list of primer information.

The qRT-PCR results shown are the averages of the three biological replicates for each primer and RNA treatment (each biological replicate being an average of three technical replicates) and the error is standard error of the mean. See Supplementary Table 2 for qRT-PCR results.

Imaging

All images were obtained on a Zeiss Axio Imager Z1 microscope with a Zeiss ApoTome attachment. Embryos were deyolked in PBS, side mounted in 80% glycerol/20% PBS and viewed with the 10×, 20× or 40× objective. For images where fluorescence levels were to be compared, exposure times were kept constant throughout the imaging of that experiment. Images were optimized by averaging up to 5 frames.

For ISH images, embryos older than 16 somites were deyolked and side mounted as above. Younger embryos were whole mounted by clearing their yolks in MeOH for 15 minutes followed by 1:2 Benzyl Alcohol:Benzyl Benzoate for 15 minutes, then dorsally orienting them in Permount. Image modifications in Adobe Photoshop were one round of linear adjustments, Gaussian filtering (0.3 pixel) and unsharp mask (50%, 1 pixel) prior to being collated in Adobe Illustrator.

Measuring myotome boundary angles

Zeiss Inside 4D software was used to calculate the angle of the chevron shaped myotome boundary from brightfield images. The angle degrees were averaged within in a treatment and then graphed and statistically analyzed for significance.

Normalized fluorescence intensity

Images were imported into ImageJ (freely available online) and the profiles were plotted. The resulting data were imported into Excel for normalization. For each panel, in order to control for varied exposure times, the maximum intensity of phalloidin was determined and

the values were all normalized to this intensity. Thus, what is shown is a "percentage of maximum intensity."

The 2D Wavelet Transform Modulus Maxima (WTMM) method

The 2D WTMM method is a multifractal image analysis formalism originally introduced in Arneodo et al., 2000 that has been adapted to perform a structural, multi-scale anisotropic analysis of image features having a complex geometry (Arnedo, 2000; Khalil, 2006). At a given scale *a*, the WTMM are defined by the positions where the Wavelet Transform Modulus is locally maximum in the direction *A* of the gradient vector. These WTMM lie on connected chains called *maxima chains*. Vectors along the maxima chains corresponding to positions where the image gradient is locally maximal on the maxima chain are the WTMM maxima, or WTMMM. Their angle indicates locally the direction where the signal has the sharpest variation.

At all size scales *a*, the probability density functions (pdfs), $P_a(A)$, of the angles, *A*, are associated to each WTMM vector. A flat pdf indicates random directions of sharpest intensity variation (*i.e*. isotropy). The *anisotropy factor*, F_a:

$$F_a = \int_{-\pi}^{\pi} \left| P_a(A) - \frac{1}{2\pi} \right| dA,$$

has been defined in such a way that a theoretically isotropic surface will have a value of $F_a = 0$, while any value greater than 0 quantifies a departure from isotropy.

Results

Characterization of nrk2b expression and morpholinos (MOs) targeting nrk2b

nrk2b is expressed in muscle tissue at 26 hpf (Thisse et al., 2004). We found that *nrk2b* expression is initiated in the paraxial mesoderm at tailbud stage (data not shown) and persists through at least 35 hpf (Fig. 1 A-A6). In order to determine the function of Nrk2b in muscle development, we designed two non-overlapping, translation-blocking MOs targeting *nrk2b* (Fig. 1 B). Injection of 12 ng of control MO did not elicit a phenotype (Fig. 1 C-C1). Injection of either 24 ng MO1 or 12 ng MO2 disrupted muscle development: myotomes were U-shaped and thinner in the anterior-posterior dimension than in controls (Fig. 1 D-D1, E-E1). Injection of half the functional amount of MO1 or MO2 did not disrupt muscle development (Fig. 1 F-F1, G-G1). Co-injection of 12 ng MO1 + 6 ng MO2 elicited the same phenotype as embryos injected with higher levels of single MOs (compare Fig. 1 H-H1 to D-D1, E-E1). This synergy suggests that these MOs disrupt translation of the same gene product (Eisen and Smith, 2008). The MO cocktail of 12 ng MO1 + 6 ng MO2 was injected in all the ensuing experiments.

A *nrk2b:gfp* fusion construct containing the MO target sequences was generated using the Tol2Kit (Kwan et al., 2007) to test the effectiveness of the *nrk2b* MO cocktail in blocking translation of Nrk2b protein. This fusion construct was injected with and without the *nrk2b* MO cocktail. *nrk2b* MOs dramatically decreased translation of the Nrk2b:GFP fusion protein in all embryos observed (Fig. 1 K-K1, 3 experiments, 1 representative experiment: 93% of *nrk2b:gfp* injected embryos expressed GFP (n=171 out of 184 embryos) whereas only 5% of *nrk2b:gfp* + *nrk2b* MO injected embryos expressed any GFP (n=1 out of 20 embryos, *nrk2b* MOs knocked down Nrk2b:GFP protein for at least 26 hours, data not shown). These data indicate that two separate, non-overlapping *nrk2b* MOs synergize and are sufficient to disrupt Nrk2b translation. Because injection of MOs can activate the p53 pathway and cause non-specific effects (Robu et al., 2007), we co-injected the *nrk2b* MO

cocktail 1:1 with *p53* MO (Robu et al., 2007). Co-injection of *p53* MO rescued necrosis in the head, but not U-shaped myotomes and shorter body axes (Fig. 1 L-N). Myotome boundary angles in *nrk2b* morphants are significantly wider than controls (Fig. 1 J, student t-test, $p < 0.001$). Myotome boundary angles in *nrk2b:p53* double morphants are also significantly wider than controls (Fig. 1 J, student t-test, $p < 0.001$) and are not significantly different than boundary angles in *nrk2b* morphants (Fig. 1 J). Thus, co-injection of *p53* MO does not rescue the paraxial mesoderm phenotype of *nrk2b* morphants.

Nrk2 was identified in a yeast two-hybrid screen for proteins that interact with the Laminin receptor Integrin α7β1 (Li et al., 1999). It was subsequently shown that ectopic Nrk2 expression in C2C12 myoblasts disrupts adhesion to Laminin, but not the ECM protein Fibronectin (Li et al., 2003). The fact that the phenonotype of the paraxial mesoderm in *nrk2b* morphants resembles that of *laminin β1* and *γ 1* mutants (Parsons et al., 2002b), in that myotomes are narrower in the anterior-posterior axis, suggests that Nrk2 may mediate adhesion to Laminin *in vivo* as well as *in vitro*. Myotome boundary angles in *laminin* mutants and *nrk2b* morphants are not significantly different (student t-test, $p = 0.3$), and both are significantly wider compared to controls (Fig. 1 J, student t-test, $p<0.001$). These data suggest that Nrk2b mediates adhesion to Laminin. However, these data do not clarify whether Nrk2b affects adhesion of muscle cells to other ECM proteins. We thus conducted pseudo-genetic epistasis analysis. Injection of *nrk2b* MOs into *laminin* mutants phenocopies *laminin* mutants (Fig. 2 A-D). This result suggests that Nrk2b participates in the Laminin signaling pathway during early development.

The preceding data provide evidence that *nrk2b* MOs are specific. First, two MOs targeting *nrk2b* generate a similar phenotype, suggesting that they disrupt translation of *nrk2b*. Second, the phenotype is recapitulated by co-injection of sub-functional doses of both MOs. Third, *nrk2b* MOs block translation of a Nrk2b:GFP fusion protein containing the target sequences for the MOs. Fourth, co-injection of *p53* MO with the *nrk2b* MO cocktail rescues the cell death seen in the head of *nrk2b* morphants, but does not rescue the disrupted muscle phenotype. Fifth, injection of *nrk2b* MOs into wild-type or *laminin γ1* mutants phenocopies the *laminin* mutant phenotype. Taken together, these results suggest that *nrk2b* MOs disrupt translation of Nrk2b protein and do not cause significant “off-target” effects (Eisen and Smith, 2008).

MTJs are disrupted in nrk2b morphants

MTJ development is disrupted by 48 hpf in *laminin β1* and *γ1* mutants (Snow et al., 2008a). Given the above data suggesting that *nrk2b* participates in Laminin signaling/adhesion, we asked whether MTJ development is also disrupted in *nrk2b* morphants. Phalloidin staining, to visualize filamentous-actin, showed organized elongated muscle fibers in 48 hpf controls (Fig. 2 E). The MTJ is the dark region devoid of actin staining (pseudocolored purple in Fig. 2 E1, F1, G, H). In contrast, about one third (71/212, 33%) of MTJs in every 48 hpf *nrk2b* morphant contained foci where MTJs were disrupted and muscle fibers were abnormally long (pseudocolored yellow in Fig. 2 F1). Approximately the same proportion of MTJs (19/67, 28%) were disrupted in all 96 hpf *nrk2b* morphants (Fig. 2 H). Similar proportions of disrupted MTJs in 48 and 96 hpf *nrk2b* morphants indicates that there is no age-dependent degeneration of the MTJ. This phenotype of disrupted MTJs is also observed in *nrk2b:p53* double morphants (data not shown). These data show that Nrk2b is required for normal muscle development and raise the question of why *nrk2b* morphant MTJs are discontinuous.

In teleosts, MTJs are derived from initial epithelial somite boundaries. Therefore, we asked if discontinuous MTJs at 48 hpf are a direct consequence of discontinuous initial somite boundary formation. Although somites are misshapen in *nrk2b* morphants, segmentally

reiterated boundaries form (Fig. 2 I, K) and the expression of somite patterning genes appears normal (Fig. 2 panels J and L). Similar to *laminin β1* and *γ1* mutants (Snow et al., 2008a), initial somites are narrower in the anterior-posterior dimension (Fig. 2 N). These abnormally shaped but continuous somite boundaries are clearly visible when phalloidin staining is used to outline cells (Fig. 2 N). In controls at 26 hpf, MTJs are clearly V-shaped and actin is slightly enriched at the terminal ends of muscle fibers attached to MTJs, (Fig. 2 O, white arrow). In contrast, actin is strikingly enriched at the terminal ends of muscle fibers at the MTJ and depleted within myotubes in 26 hpf *laminin γ1* mutants (Fig. 2 P). Similar actin distribution is observed in both *nrk2b* morphants and *nrk2b* MO-injected *laminin γ1* mutants (Fig. 2 Q and R, respectively). These differences in actin distribution are clear when normalized fluorescence intensity in the anterior-posterior dimension is graphed (see methods) (Fig. 2 O-R). Note that the peaks and valleys of fluorescence intensity in controls (Fig. 2 O) are less extreme than those in the other panels (Fig. 2 P-R). These data suggest that adhesion to Laminin may be required for normal cellular distribution of F-actin. In addition, this higher resolution analysis of *nrk2b* morphant-*laminin γ1* mutants indicates that injection of *nrk2b* MOs into *laminin γ1* mutants does slightly affect the *laminin* mutant phenotype. Boundaries are more U-shaped than *laminin γ1* mutants injected with control MO (compare Fig. 2 P and R). Both *laminin β1* and *laminin γ1* are maternally expressed (Parsons et al., 2002b), and we have found that injection *of laminin γ1* MOs into *laminin γ1* mutants results in early embryonic lethality (data not shown). We hypothesize that injection of *nrk2b* MOs into *laminin γ1* mutants disrupts adhesion to maternally provided Laminin and thus results in a slightly worse phenotype. Taken together, these data indicate that discontinuous MTJs at 48 hpf in *nrk2b* morphants are not due to discontinuous somite boundary formation earlier in development. In addition, these data further show that the *nrk2b* morphant phenotype resembles that of *laminin* mutants, supporting the hypothesis that Nrk2b functions in Laminin-mediated adhesion/signaling.

Exogenous NAD+ rescues MTJ deterioration in nrk2b morphants

Yeast and human Nrk2 phosphorylate Nicotinamide Riboside to generate NAD+ through an alternative salvage pathway (Bieganowski and Brenner, 2004). Zebrafish embryos lacking Nrk2b are therefore potentially deficient in NAD+. We hypothesized that addition of exogenous NAD+ would rescue the *nrk2b* morphant phenotype. We incubated control and *nrk2b* MO-injected embryos in 100 μM or 1 mM exogenous NAD+ beginning at shield stage (see methods). Addition of NAD+ to control MO-injected embryos did not affect muscle development (Fig. 3 A). Body axes are again shorter, somites are U-shaped, and MTJs are discontinuous in *nrk2b* morphants (Fig. 3 panels B). Exogenous NAD+ rescued the *nrk2b* morphant paraxial mesoderm phenotype. Morphants incubated in 100 μM or 1 mM NAD+ had longer body axes and greatly decreased boundary angles that were significantly different from angles in *nrk2b* morphants (Fig. 3 panels C, D and E, $p < 0.001$ for both concentrations). Approximately 7% of MTJs were discontinuous in morphants treated with 100 μM NAD+ (Fig. 3 C2). Discontinuous MTJs in NAD+-treated *nrk2b* morphants with normal boundary angles indicate that MTJ disruption is not a nonspecific side effect of wider MTJs. Although myotome boundary angles were not significantly different in *nrk2b* morphants grown in 100 μM and 1 mM NAD+, there was a difference in MTJ integrity. Far fewer MTJs were discontinous in morphants treated with 1 mM NAD+ than treated with 100 μM NAD+ (Fig. 3 F). Thus, there is a dose-dependent rescue of MTJ integrity when *nrk2b* morphants are supplemented with NAD+. Treatment of *laminin* mutants with exogenous NAD+ did not rescue wider myotome boundary angles or MTJ crossings (Fig 3 E, F, H, and I). Taken together, these data suggest that the main role of Nrk2b in muscle morphogenesis is to generate NAD+ and that NAD+ production is functionally upstream of Laminin adhesion/signaling.

Nrk2b is required non-cell autonomously for basement membrane polymerization at the MTJ

We showed that discontinuous MTJs in *nrk2b* morphants at 48 hpf are not due to discontinuous somite boundaries. Somite boundary morphogenesis into nascent MTJs occurs around 24 hpf (Henry et al., 2005) and polymerized Laminin-111, indicative of basement membrane assembly, robustly concentrates throughout the MTJ at this time (Crawford et al., 2003; Snow and Henry, 2008). We asked if Nrk2b is required for basement membrane formation because Nrk2b interacts specifically with the Laminin receptor, Integrin α7β1, *in vitro* (Li et al., 2003). In controls, Laminin-111 at the basement membrane is clear as a distinct line between adjacent myotomes (Fig. 4 A1-3, small square panels). In 3D projections, the organization and continuous nature of Laminin-111 in the medial-lateral dimension is clear (Fig. 4 A1-3, large square panels). When the 3D projections are rotated to generate a transverse view, high levels of Laminin-111 are observed throughout the medial-lateral extent of the MTJ except for the horizontal myoseptum (dark vertical line, Fig. 4 A1-3, tall rectangular panels, Laminin is observed at the MTJ adjacent to slow-twitch fibers in blue, but also medially in the fast-twitch muscle domain). In contrast, the MTJ basement membrane in *nrk2b* morphants is disorganized and discontinuous. At a lower magnification view, Laminin-111 at the MTJ in *nrk2b* morphants appears similar to controls (compare Fig. 4 A to B). Upon closer inspection, however, it is clear that Laminin-111 is not laid down in a straight and organized line (Fig. 4 B1-3, small square panels). The basement membrane is not always continuous, i.e. there are holes in Laminin-111 at the MTJ (Fig. 4 B3, white arrow in large square panel, note gap in Laminin-111 staining in the top left small square panel, this gap appears as a hole in Laminin-111 staining when 3D projected, see Supplemental movies). These holes do not represent gaps within muscle tissue because staining for phalloidin, which outlines cells, showed that muscle fibers terminated adjacent to the gaps/holes (Fig. 4 B3, white arrow in small square panel). This disorganization of the basement membrane is especially clear in 3D projections (Fig. 4 B1-3, large square panels). The transverse view shows that levels of Laminin-111 are not uniform throughout the medial-lateral extent of the MTJ (Fig. 4 B1-3, tall rectangular panels). Interestingly, Laminin-111 deposition appears to be particularly poor in the MTJ adjacent to the medial fast-twitch muscle domain (Fig. 4 B1-3, tall rectangular panels).

The above data indicate that basement membrane assembly at the MTJ is disrupted in *nrk2b* morphants. To test whether this disruption is a common phenotype when adhesion to Laminin-111 is disrupted, we assayed basement membrane assembly in *dystroglycan* morphants. Dystroglycan is a component of the Dystrophin-Glycoprotein Complex (DGC), a transmembrane receptor for Laminin, and is crucial for maintenance of muscle fiber attachment to the ECM. It has previously been shown that *dystroglycan* morphants have muscular dystrophy (Parsons et al., 2002a), but the age of onset has not been closely investigated. We find that MTJs in *dystroglycan* morphants at 26 hpf are fairly normal (Fig. 4 C). Very few MTJs are discontinuous and crossed by abnormally long muscle fibers (2 experiments, 13 embryos, 4/110 MTJs crossed). Careful inspection of the basement membrane in *dystroglycan* morphants corroborates this conclusion. 3D and transverse projections show robust basement membrane polymerization (Fig. 4 panels C). Even when the MTJ is discontinuous and there is a hole in the basement membrane that is crossed by muscle fibers, the adjacent basement membrane is robust (Fig. 4 C1, square panels, red arrowhead). Importantly, transverse views show that basement membrane assembly in the fast-twitch muscle domain is robust adjacent to the gap in the MTJ that is crossed by muscle fibers (Fig. 4 C1, tall rectangular panel, red arrowhead).

By applying the 2D Wavelet Transform Modulus Maxima (WTMM) method (Arnedo, 2000; Khalil, 2006; Snow et al., 2008a; Snow et al., 2008b) we performed a structural, multi-scale anisotropy analysis to rigorously and objectively assess CMAC components at the MTJ in

nrk2b morphants. The 2D WTMM method can be used to quantify the amount of structure (order) of objects that do not have a well-defined boundary (see methods) by calculating the angle of steep gradients in pixel intensity, at different size scales. This is perhaps most apparent in controls, where most of the arrows plotting this angle are parallel to each other (Fig. 4 panels E). Angles are also mostly parallel in *dystroglyan* morphants (Fig. 4 panels F). However, arrows are far less organized in *nrk2b* morphants (Fig. 4 panels G). This organization is quantified by calculating the probability density function of the angles, from which we obtain the anisotropy factor (see methods). The anisotropy factor is the departure from isotropy or randomness. A higher anisotropy factor indicates a more ordered structure. We found that control and *dystroglycan* morphants have similar anisotropy factors (Fig. 4 D). The anisotropy factor of Laminin-111 staining in *nrk2b* morphants is significantly lower, indicating a more random structure (student t-test, $p < 0.01$, Fig. 4 D). These data indicate that Nrk2b is required for normal basement membrane assembly.

Possible explanations for the apparent decrease in Laminin-111 at *nrk2b* morphant MTJs are: (1) reduced *laminin* transcription, (2) increased Laminin-111 degradation or (3) less efficient assembly/polymerization of Laminin-111. We used multiple experimental approaches to distinguish between these possible mechanisms. We first analyzed *laminin* transcription at 24 hpf because this is the earliest time that basement membranes at the MTJ are reliably robust in controls and disrupted in *nrk2b* morphants. Neither of these *laminin* chains is highly expressed in controls at 24 hpf (Fig. 5 B, C). Expression of both chains appears increased in 24 hpf *nrk2b* morphants (Fig. 5 B1, C1). Because expression levels are somewhat low, we also quantitatively analyzed transcription of the three *laminin* chains that make up Laminin-111. Comparative quantitative Reverse Transcriptase-Polymerase Chain Reaction (qRT-PCR) of controls and *nrk2b* morphants indicated that these three *laminin* chains are not downregulated in *nrk2b* morphants (Fig. 5 A). If anything, transcription of these *laminin* chains is increased. Transcription of *laminin α1* is upregulated approximately 2.5 fold compared to controls. Because all three chains are required for Laminin-111 assembly, it is not clear whether dramatically increased transcription of one chain affects levels of Laminin-111 protein (we have been unsuccessful at using Westerns to detect Laminin-111 with the above antibody, this is probably due to the fact that the antibody recognizes assembled and polymerized Laminin-111). However, these data allow us to conclude that the disruption in Laminin-111 at the MTJ basement membrane is not due to decreased *laminin* transcription.

Another mechanism that could account for the holes in the MTJ basement membrane in *nrk2b* morphants is increased degradation of Laminin-111. We used genetic mosaic analysis to ask whether *nrk2b* morphant cells are sufficient for Laminin-111 degradation. Nrk2b-deficient cells were transplanted into wild-type hosts and the MTJ basement membrane was assessed at 48 hpf. No holes in the MTJ basement membrane were observed adjacent to Nrk2b-deficient cells in control hosts (Fig. 5 D-D3, $n = 68$ cells). We also asked whether Nrk2b-deficient cells were able to elongate across MTJ boundaries. Only 9/485 (2%) cells crossed control MTJ boundaries (Fig. 5 E). Genetic mosaic analysis of myotubes is complicated by their multinucleate nature. However, we can conclude that Nrk2b-deficient cells are not sufficient, even in large quantities, to frequently induce Laminin degradation. Taken together, the above data suggest that Nrk2b is non-cell autonomously required for basement membrane polymerization and that basement membrane polymerization is a phenomenon mediated by communities of cells. To our knowledge, this is the first example of an intracellular protein critical for basement membrane assembly during muscle development *in vivo*.

The percentage of holes in Laminin-111 at 24 hpf is similar to the percentage of MTJs crossed at 48 hpf (Fig. 5 E). Muscle integrity does not degenerate through time in *nrk2b*

morphants: the percentage of MTJs crossed at 96 hpf is similar to the percentage crossed at 48 hpf (Fig. 5 E). These results suggest that initial defects in basement membrane assembly precede muscle fibers crossing through the defective basement membrane later in development, resulting in discontinuous MTJs (Fig. 5 F).

CMAC assembly is aberrant in nrk2b morphants

The above data show that Laminin-111 is not efficiently polymerized at the MTJ basement membrane in *nrk2b* morphants. Recruitment of intracellular scaffolding and signaling proteins, like Focal Adhesion Kinase (FAK), Paxillin and β-Dystroglycan, to CMACs is critical for the assembly and maintenance of the ECM (Lock et al., 2008; Lunt et al., 2009; White et al., 2008). Thus, we assessed CMAC assembly at the MTJ both qualitatively and quantitatively, with the WTMM formalism. The WTMM formalism was applied to images for β-Dystroglycan, pY861 FAK, pY397 FAK, and Paxillin. In order to best assess structure at the MTJ, we analyzed wavelets between 1.88 and 3.75 μm. β-Dystroglycan robustly concentrates at the MTJ in controls at 26 hpf (Fig. 6 A, white arrows). This organized staining is reflected in a relatively high anisotropy factor, approximately 1.3, across all size scales analyzed (Fig. 6 M, dark blue bars). β-Dystroglycan concentrates at *nrk2b* morphant MTJs, but is slightly less robust than in controls (Fig. 6 B, ct n=31 MTJs, *nrk2b* MOs n=44 MTJs). This difference is clear when the anisotropy factor is calculated (Fig. 6 M, light blue bars): β-Dystroglycan is significantly less organized in *nrk2b* morphants for all size scales examined ($p < 0.001$). Both FAK (data not shown, ct n=48 MTJs; *nrk2b* MOs n=43 MTJs) and tyrosine phosphorylated FAK concentrated at the MTJ in controls and *nrk2b* morphants (Fig. 6 C-F, white arrows, pY861 FAK ct n=52 MTJs, *nrk2b* MOs n=75 MTJs; pY397 FAK ct n=55 MTJs, *nrk2b* MOs n=83 MTJs). Gaps in FAK staining in *nrk2b* morphants correlated with gaps in MTJs and abnormally long muscle fibers (Fig. 6 D, F, red arrows). Anisotropy factors reflecting organization of pY FAK between control and *nrk2b* morphants were more similar to each other, but still significantly different (Fig. 6 N, O, p values ranged from 0.02 to 0.05, there was no correlation of size scale with p value). These results indicate that although concentration of β-Dystroglycan and pY FAK appear qualitatively similar to controls, subcellular localization of these proteins at the MTJ is less organized in *nrk2b* morphants than in controls.

Strikingly, the localization of a different CMAC component, Paxillin, was disrupted in all *nrk2b* morphants analyzed (Fig. 6 G-H, imaging parameters were the same for controls and morphants, ct n=200 MTJs; *nrk2b* MOs n=181 MTJs). Note that Paxillin is concentrated at MTJs in controls, but is not highly concentrated at the MTJ in *nrk2b* morphants. Interestingly, similar to Laminin-111 staining, Paxillin staining at the MTJ within slow-twitch muscle fibers was not affected (data not shown), but was disrupted in the more medial fast-twitch fiber domain. The anisotropy factor was strikingly lower for *nrk2b* morphants than controls over all size scales (Fig. 6 P, $p < 0.001$). In controls, the anisotropy factors for pY FAK and Paxillin are not significantly different (Fig. 6 Q). In contrast, the anisotropy factor for Paxillin in *nrk2b* morphants was significantly different than pY FAK ($p < 0.01$). Addition of exogenous NAD+ rescues Paxillin concentration at the MTJ in the medial fast-twitch muscle domain in *nrk2b* morphants (Fig. 6 U–W). Taken together, the qualitative and quantitative assessments of CMAC formation in *nrk2b* morphants indicate that Paxillin concentration at MTJ CMACs is dramatically disrupted in *nrk2b* morphants.

The lack of robust Paxillin concentration at MTJs in *nrk2b* morphants could be due to: (1) decreased *paxillin* transcription, (2) less Paxillin protein or (3) reduced recruitment/retention of Paxillin to MTJ CMACs. qRT-PCR for *paxillin* transcript levels show that *paxillin* transcription is normal in *nrk2b* morphants (Fig. 6 R). Densitometry measurements of Paxillin antibody staining and Western analysis suggested that there is not a reduction in Paxillin protein in *nrk2b* morphants (Fig. 6 S, T, respectively). One caveat, however, is that

densitometry is qualitative and qRT-PCR and Westerns represent levels within entire embryos. Thus, although it does not appear to be the case, there could be a physiologically significant reduction of Paxillin levels in muscle tissue. These data suggest the hypothesis that Nrk2b is required for recruitment and/or retention of cytoplasmic Paxillin to MTJ CMACs.

The above data indicate a specific requirement for Nrk2b in Paxillin localization at MTJ CMACs. This represents a novel model system with which to ask important questions about CMAC assembly *in vivo*. We used genetic mosaic analysis to ask whether Paxillin localization to MTJ CMACs was restored in wild-type cells transplanted into *nrk2b* morphants. Normal β-Dystroglycan localization indicated that cells are not appreciably perturbed by transplantation (Fig. 7 panels B). Similar results were obtained when pY397 FAK concentration at the MTJ was analyzed (Fig. 7 panels C). Strikingly, Paxillin localization to MTJs was rescued in wild type cells, but not in the Nrk2b-deficient cells surrounding them (Fig. 7 panels D) The multinucleate nature of fast-twitch muscle fibers and the possibility that wild-type cells fused with Nrk2b-deficient cells implies that even reduced amounts of Nrk2b are sufficient for Paxillin concentration at the MTJ. This result indicates that the protein composition of CMACs can be modulated cell autonomously *in vivo*.

Paxillin is sufficient for boundary capture in nrk2b morphants

The data thus far suggest multiple hypotheses, including: (1) Paxillin concentration at the MTJ promotes normal basement membrane assembly and boundary capture, (2) Paxillin concentration at the MTJ is a read-out of robust CMAC assembly, (3) adhesion to Laminin-111 is critical for Paxillin concentration at the MTJ, or (4) Paxillin concentration at the MTJ and basement membrane assembly are linked through inside-out and outside-in signaling. Unfortunately we do not currently possess the tools for dynamic, *in vivo* analysis of basement membrane assembly and are unable to definitively discriminate between these hypotheses. However, analysis of Paxillin subcellular localization in *laminin* mutants could be informative. If Paxillin concentrates at the MTJ in *laminin β1* mutants, hypotheses (2) and (3) could be eliminated. β-Dystroglycan concentrates at the MTJ in *laminin β1* mutants as previously reported (Fig. 8 B, Parsons et al., 2002). We find that Paxillin concentration at the MTJ is nearly abrogated in *laminin β1* mutants (Fig. 8 D). This result suggests that Paxillin concentration to the MTJ is functionally downstream of Laminin.

We asked whether overexpression of Paxillin was sufficient to rescue the *nrk2b* morphant phenotype using a transgenic line that ubiquitously overexpresses Paxillin:GFP. Paxillin:GFP concentrates robustly at MTJs in control transgenic embryos and Paxillin overexpression does not disrupt early development (data not shown). Interestingly, Paxillin:GFP also robustly concentrates at MTJs in transgenic embryos injected with *nrk2b* MOs. Overexpression of Paxillin:GFP did not significantly decrease wider MTJ angles in *nrk2b* morphants (Fig. 8 G, student t-test, $p=0.17$). However, overexpression of Paxillin:GFP did significantly reduce the percentage of MTJs crossed by muscle fibers in *nrk2b* morphants (Fig. 8 H, student t-test, $p< 0.01$). These data indicate that MTJ angle and MTJ integrity can be uncoupled. Furthermore, these data implicate Paxillin as a major regulator of boundary capture *in vivo*.

Discussion

Signaling through cell adhesion complexes not only mediates cell migration and cell shape changes, but also influences all other major cellular functions. Thus, these complexes are best thought of as flexible and dynamic information handling machines (Lock et al., 2008). Elucidating how adhesion complexes mediate the cellular and molecular mechanisms

underlying myotube formation and tendon attachment is critical to understanding musculoskeletal development and the transition to disease states. We show that a novel protein, Nrk2b, is required for muscle development *in vivo*. Importantly, we identify Nrk2b functions at the tissue, cellular and molecular levels (Fig. 9). Nrk2b is required for normal basement membrane assembly at the MTJ. In the absence of Nrk2b, MTJs are discontinuous, resulting in abnormally long muscle fibers. Nrk2b also regulates the molecular composition of CMACs. Nrk2b is required for normal FAK and β-Dystroglycan organization at the MTJ and localization of Paxillin to the MTJ is nearly abolished in *nrk2b* morphants. Finally, we provide evidence that the molecular function of Nrk2b is NAD+ production: addition of exogenous NAD+ rescues the *nrk2b* morphant phenotype. Multiple lines of evidence suggest that Nrk2, although little studied, is a highly significant protein with important functions in muscle growth and disease. Microarray analysis of "double muscled" *myostatin* −/− cows found that *itgβ1bp3/nrk2* is the second most upregulated muscle transcript, second only to *troponin T type 1*. *nrk2* transcription is also highly upregulated in alveolar soft-part sarcoma (Stockwin et al., 2009), a rare and highly metastatic cancer with poor prognosis. These data do not determine whether *nrk2* upregulation is a cause or an effect of increased muscle growth/proliferation. However, they do suggest that *in vivo* functional analysis may identify conserved functions of Nrk2 with therapeutic relevance.

A novel morphogenetic role for NAD+

NAD+ is a ubiquitous coenzyme best known for its role in metabolic electron transfer reactions, but is also a critical coenzyme for many different reactions. For example, NAD+ is an obligatory substrate in ADP-ribosylation reactions that influence processes ranging from DNA repair to cell signaling and adhesion (Hassa and Hottiger, 2008; Kahn, 2009; Keppler and Archer, 2008; Koch-Nolte et al., 2008; Myers and Casanova, 2008; Sabe et al., 2006; Saporita et al., 2007). Although recent data have identified a novel NAD(H) binding protein that links metabolic cues with cell cycle regulation, roles for NAD+ during morphogenesis have not been identified. We show that Nrk2b regulates morphogenesis by production of NAD+. It was traditionally thought that the only mechanism for NAD+ synthesis was *de novo* synthesis from amino acids. Within the last decade, however, an alternative salvage pathway that generates NAD+ has been identified (Bieganowski and Brenner, 2004). This pathway involves salvage of Nicotinic acid, Nicotinamide, or Nicotinamide Riboside (Belenky et al., 2009; Tempel et al., 2007). Nicotinamide Riboside Kinases, Nrks, phosphorylate Nicotinamide Riboside, a critical step towards NAD+ synthesis. The question that remains, however, is how NAD+ regulates morphogenesis. Because a role for NAD+ during morphogenesis has not previously been shown, we can only speculate. We hypothesize that Nrk2b post-translationally promotes basement membrane assembly by providing a local source of NAD+ used to ADP-ribosylate Integrins. ART1 is an ecto-mono-ADP-ribosylatransferase that ADP-ribosylates Integrin α7 at multiple sites, depending upon NAD+ concentration (Zhao et al., 2005; Zolkiewska and Moss, 1997). This ADP-ribosylation by ART1 is not readily reversible and leads to an increased Laminin-binding affinity of Integrin α7β1 in differentiated myotubes. Given that NAD+ is an obligatory substrate in ADP-ribosylation reactions, the authors hypothesized that Integrin α7 ADP-ribosylation might be a protective mechanism that increases Integrin α7β1 adhesion to Laminin when the sarcolemma has been compromised and intracellular NAD+ leaks into the extracellular space. However, it is also possible that Integrin ADP-ribosylation and the subsequent increased affinity for Laminin is a morphogenetic mechanism that promotes basement membrane polymerization. We have identified two ART1 orthologues expressed in developing zebrafish skeletal muscle (unpublished data). Preliminary data indicate that expression of these ARTs is Nrk2b dependent, they are required for basement membrane assembly, and act within the same pathway as Nrk2b

(Peterson and Henry, unpublished data). Thus, one interesting avenue of research is development of tools that would allow visualization of ADP-ribosylation and basement membrane assembly *in vivo*. This model is clearly very speculative. However, two recent findings establish some precedent for compartmentalized NAD+ usage and NAD+-dependent enzymes in morphogenesis. Transgenic *Arabidopsis* expressing reporter constructs for three NAD+ kinases, or NADKs, show tissue specific expression (Waller et al., 2010). Expression of GFP-tagged versions of the NADKs in suspension cultures showed that one of the three localized to the peroxisomal matrix (Waller et al., 2010). These data suggest that localized NAD+ usage may play roles in plant development and/or physiology. Data that potentially implicate NAD+ in morphogenesis were obtained by identifying a potential locus underlying isolated congenital nail clubbing (ICNC). ICNC is a rare autosomal recessive disorder characterized by abnormal connective tissue growth and matrix that lead to enlargement of digit terminal segments (Tariq et al., 2009). In one large Pakistani family, a nonsense mutation in the gene encoding NAD+-dependent 15-hydroxyprostoglandin degydrogenase is thought to underlie ICNC (Tariq et al., 2009). Taken together, our findings implicating NAD+ in morphogenesis, as well as clear roles for NAD+ in modulating Integrin affinity for Laminin in cell culture, localized usage of NAD+ in *Arabidopsis*, and roles for a NAD+-dependent enzyme in a connective tissue disease all suggest that NAD+ may be a little recognized yet important morphogenetic mediator.

Dynamic reciprocity and musculoskeletal homeostasis

Adhesion of muscle cells to the surrounding basement membrane is one of the most important aspects of musculoskeletal structure. When genes whose protein products are involved in muscle cell-basement membrane adhesion are mutated, myopathies can occur. Zebrafish models of muscular dystrophies have both validated the model and provided novel insights into pathogenesis (Bassett, 2003; Bassett, 2003; Hall, 2007; Nixon, 2005; Parsons, 2002; Postel, 2008; Steffen, 2007; Thornhill, 2008). One important insight is that the MTJ is a major site of failure in *sapje/dystrophin* mutants (Bassett, 2003). It has also recently been shown that muscle fibers detach from the basement membrane at the MTJ *prior* to membrane disruption and apoptosis in *candyfloss/laminin α2* mutants (Hall, 2007). One less appreciated but critically important aspect of musculoskeletal homeostasis is initial MTJ morphogenesis. Multiple studies have shown that disruption of ECM at the MTJ can result in the formation of aberrant and discontinuous MTJs (Snow, 2008a; Kudo, 2004; Pagnon-Minot, 2008; Snow, 2008b). In this study, we elucidate some of the underlying mechanisms that govern ECM remodeling and allow cells to integrate signaling and differentiation with the structure of their local microenvironment. This dynamic, bidirectional relationship between cells and their local ECM environment mediate basement membrane assembly at the MTJ and reinforces muscle fiber-MTJ adhesion. We show that Nrk2b, via production of NAD+, plays a critical role in basement membrane assembly. This is a novel mechanism of “inside-out” signaling. We also show that Laminin itself is critical for recruitment of Paxillin to cell-matrix adhesion complexes at the MTJ – “outside-in” signaling. Overexpression of Paxillin:GFP promotes boundary capture and termination of muscle fiber elongation, representing another example of “inside-out” signaling. These results provide a mechanistic framework for future studies investigating the positive feedback loop between cells and their matrix that reinforces and stabilizes muscle fiber-MTJ adhesion.

Nrk2b and specificity of cell adhesion function

Although it is not known how CMACs regulate disparate cellular processes such as motility, stable adhesion, proliferation, survival and invasion, it is likely that changes in their size, localization, stability and molecular composition mediate different cellular outputs. Recent advances in imaging technology (fluorescent speckle microscopy, spatio-temporal image correlation spectroscopy) have allowed new insights into the CMAC to F-actin linkage *in*

vitro (Lock et al., 2008). However, analysis of the molecular composition and size of CMACs during development is difficult, if not impossible. Analysis of the phenotypes of mice, *Xenopus* and zebrafish deficient for different CMAC components have increased understanding of CMAC function during development. These studies show that one mechanism contributing to CMAC functional specificity is tissue-restricted expression of CMAC components. But what about a CMAC component such as Paxillin, which is ubiquitously expressed during zebrafish development (Crawford et al., 2003)? How is Paxillin function within CMACs modulated in different contexts? Here, we provide one paradigm by which specificity can be achieved. We show that *nrk2b* is expressed in axial skeletal muscle and is required for Paxillin localization to MTJ CMACs. Our data do not indicate whether Nrk2b is required for Paxillin recruitment or retention/stabilization of Paxillin at MTJs. Interestingly, we also provide evidence that Nrk2b-mediated Paxillin concentration is modulated in a cell autonomous fashion. To our knowledge, this is the first mechanistic understanding of cell autonomous CMAC molecular composition regulation *in vivo*. Given the absolutely critical role of Paxillin in mediating cell adhesion and migration *in vitro* (Deakin and Turner, 2008), it is perhaps not surprising that Paxillin localization to the MTJ can be modulated in a tissue-specific manner. Importantly, the fact that Nrk2b was shown to regulate the protein level and tyrosine phosphorylation of Paxillin in C2C12 myoblasts (Li et al., 2003) suggests some conservation of Nrk2b function. Thus, an *in vivo* model of Nrk2b function may provide relevant insights into human health and disease.

Basement membranes, primarily composed of Laminin, are specialized compartments within the ECM that provide mechanical support and regulate multiple cellular activities. Laminins are heterotrimeric proteins composed of an α, β and γ chain. It is thought that once assembled, most Laminins polymerize via interactions between the three N terminal short arms (Tzu and Marinkovich, 2008). The mechanisms that regulate Laminin polymerization *in vivo* are not well understood. We show that despite normal/increased levels of *laminin* chain transcription, the MTJ basement membrane is significantly disorganized in *nrk2b* morphants. The fact that *nrk2b* morphant cells in control hosts are unable to induce basement membrane defects indicates that basement membrane assembly at the MTJ is a community-mediated phenomenon. This result suggests that the basement membrane is not disorganized because of unusually high degradation in *nrk2b* morphants. If *nrk2b* deficiency results in increased matrix proteolysis, one would predict that large cohorts of *nrk2b*-deficient cells in control hosts would be sufficient to induce basement membrane disruption. Thus, taken together, these data suggest that Nrk2b is a novel regulator of basement membrane assembly during early MTJ morphogenesis.

Paxillin at the MTJ is not required for subcellular localization of FAK to the MTJ

Paxillin and FAK were among the first identified focal adhesion proteins and, as such, the focus of thousands of studies elucidating their molecular structure and function. FAK has a central kinase domain and a C-terminal domain that targets FAK to focal adhesions. Paxillin is a scaffolding protein replete with protein-protein binding domains: SH2 and SH3 domain binding sites, four C-terminal LIM domains, and five N-terminal LD motifs (Turner and Miller, 1994). Paxillin and FAK directly interact and FAK phosphorylation and localization to focal adhesions are reduced in *paxillin* −/− cells (Hagel et al., 2002; Wade et al., 2002). LD motifs 2 and 4 of Paxillin bind to the α-helix 1/4 and α -helix 2/3 Paxillin binding sites within the Focal Adhesion Targeting (FAT) domain of FAK (Bertolucci et al., 2005; Gao et al., 2004; Thomas et al., 1999). A recent *in vitro* study analyzed the function of these two Paxillin binding sites within FAK. In the absence of both sites, only about 10% of FAK localizes to focal adhesions. The presence of either Paxillin-binding site is sufficient for FAK targeting to focal adhesions. However, both Paxillin-binding sites are necessary for maximal FAK activation and phosphorylation of downstream substrates (Scheswohl et al.,

2008). Given these *in vitro* data, it is curious that FAK phosphorylation and concentration at the MTJ are not more disrupted in *nrk2b* morphants that show disrupted Paxillin. In this regard, there is evidence from *in vitro* studies that secondary mechanisms for FAK subcellular localization may exist. Notably, although glutamic acid 997 of FAK does not normally play a role in FAK localization to focal adhesions, this residue is required for FAK localization to focal adhesions when FAK binding to Paxillin is abrogated (Scheswohl et al., 08). Thus, it is possible that within the complex *in vivo* environment, there are multiple mechanisms mediating FAK concentration at CMACs. Alternatively, it is possible that FAK at the MTJ is primarily localized to the Dystrophin-Glycoprotein Complex (DGC) that also anchors the intracellular cytoskeleton to Laminin in the ECM. Far less is known about dynamics of DGC assembly and it is not known if Paxillin is required for FAK recruitment to DGC based adhesions. Regardless, our data show that normal Paxillin localization is not required for robust concentration of FAK to CMACs at the MTJ *in vivo*.

Quantitative analysis of morphogenesis

The ability to quantify phenotypes is critical when investigating development or disease. A mathematical approach facilitates both an understanding of experimental/developmental variability and also aids in identifying subtle differences that could otherwise be construed as noise (Cooper and Albertson, 2008). For example, morphometric analyses determined that adult zebrafish haploinsufficient for Fgf8 have craniofacial defects (Albertson and Yelick, 2007). The authors posit that one approach to identifying later developmental roles for homozygous lethal mutations is to quantitatively analyze morphogenesis in heterozygous embryos. Quantification is also important for comparing the efficacy of different treatments in animal models of disease. Towards this end, the minimal “Feret’s diameter” has been identified as an excellent tool for reliable measure of fiber size in *mdx* −/− mice (Briguet et al., 2004). Multiple laboratories have developed excellent methodologies for quantification of morphogenesis (Park et al., 2008; Yin et al., 2008). In this manuscript, we used the 2D WTMM method (Arneodo et al. 2000; Khalil et al. 2006; Snow et al. 2008a, b; Khalil et al. 2009) to characterize the anisotropic signature (order/structure) of muscle architecture. Use of the 2D WTMM formalism showed that the basement membrane at the MTJ is significantly less organized in *nrk2b* morphants than in control or *dystroglycan* morphants. Importantly, however, we also showed that the 2D WTMM can be invaluable in parsing out subtle differences in CMAC organization. Although recruitment of both pY FAK and β-Dystroglycan to the MTJ appears normal in *nrk2b* morphants, there is a significant difference in CMAC organization.

Conclusions

Zebrafish axial muscle development is an ideal paradigm for quantitatively integrating functions for cell adhesion in morphogenesis. We show that Nrk2b-mediated NAD+ production regulates basement membrane assembly and boundary capture at the MTJ, Nrk2b indirectly regulates Paxillin concentration at the MTJ, and exogenous Paxillin expression is sufficient to rescue boundary capture in *nrk2b* morphants. Thus, we have identified novel roles for NAD+ during morphogenesis and for Paxillin during boundary capture *in vivo*. Taken together, these data provide novel insight into contributions of cell adhesion to morphogenesis.

Supplementary Material

Refer to Web version on PubMed Central for supplementary material.

Acknowledgments

The authors would like to thank all present and former members of the Henry Lab, especially Molly Jenkins for generation of the Paxillin:GFP transgenic zebrafish line and Nrk2b:GFP construct, Judi Azevedo for help with qRT-PCR experiments, Susannah Orzell for initial MO dosing guidelines, Mary Astumian for performing Western blots, Erik McCarthy for *in silico* analysis of MIBP2/Nrk2/ITGB1BP3 and Matthew Peterson for sharing preliminary ecto-mono-ADP-ribosyltransferase data. Additional thanks goes to Emily Notch, Greg Mayer, the Kim Lab and Mary Tyler. This work was supported by NIH grant RO1 HD052934.

References

Albertson RC, Yelick PC. Fgf8 haploinsufficiency results in distinct craniofacial defects in adult zebrafish. Dev Biol. 2007; 306:505–515. [PubMed: 17448458]

Arnedo A. A wavelet-based method for multifractal image analysis. I. Methodology and test applications on isotropic and anisotropic random rough surfaces. European Journal of Physics B. 2000; 15:567–600.

Belenky P, Bogan KL, Brenner C. NAD+ metabolism in health and disease. Trends Biochem Sci. 2007a; 32:12–19. [PubMed: 17161604]

Belenky P, Christensen KC, Gazzaniga F, Pletnev AA, Brenner C. Nicotinamide Riboside and Nicotinic Acid Riboside Salvage in Fungi and Mammals: QUANTITATIVE BASIS FOR Urh1 AND PURINE NUCLEOSIDE PHOSPHORYLASE FUNCTION IN NAD+ METABOLISM. J Biol Chem. 2009; 284:158–164. [PubMed: 19001417]

Belenky P, Racette FG, Bogan KL, McClure JM, Smith JS, Brenner C. Nicotinamide riboside promotes Sir2 silencing and extends lifespan via Nrk and Urh1/Pnp1/Meu1 pathways to NAD+ Cell. 2007b; 129:473–484. [PubMed: 17482543]

Bertolucci CM, Guibao CD, Zheng J. Structural features of the focal adhesion kinase-paxillin complex give insight into the dynamics of focal adhesion assembly. Protein Sci. 2005; 14:644–652. [PubMed: 15689512]

Bieganowski P, Brenner C. Discoveries of nicotinamide riboside as a nutrient and conserved NRK genes establish a Preiss-Handler independent route to NAD+ in fungi and humans. Cell. 2004; 117:495–502. [PubMed: 15137942]

Bissell MJ, Hall HG, Parry G. How does the extracellular matrix direct gene expression? J Theor Biol. 1982; 99:31–68. [PubMed: 6892044]

Bogan KL, Brenner C. Nicotinic acid, nicotinamide, and nicotinamide riboside: a molecular evaluation of NAD+ precursor vitamins in human nutrition. Annu Rev Nutr. 2008; 28:115–130. [PubMed: 18429699]

Briguet A, Courdier-Fruh I, Foster M, Meier T, Magyar JP. Histological parameters for the quantitative assessment of muscular dystrophy in the mdx-mouse. Neuromuscul Disord. 2004; 14:675–682. [PubMed: 15351425]

Chatzizacharias NA, Kouraklis GP, Theocharis SE. Clinical significance of FAK expression in human neoplasia. Histol Histopathol. 2008; 23:629–650. [PubMed: 18283648]

Cooper WJ, Albertson RC. Quantification and variation in experimental studies of morphogenesis. Dev Biol. 2008; 321:295–302. [PubMed: 18619435]

Crawford BD, Henry CA, Clason TA, Becker AL, Hille MB. Activity and distribution of paxillin, focal adhesion kinase, and cadherin indicate cooperative roles during zebrafish morphogenesis. Mol Biol Cell. 2003; 14:3065–3081. [PubMed: 12925747]

Deakin NO, Turner CE. Paxillin comes of age. J Cell Sci. 2008; 121:2435–2444. [PubMed: 18650496]

Digman MA, Brown CM, Horwitz AR, Mantulin WW, Gratton E. Paxillin dynamics measured during adhesion assembly and disassembly by correlation spectroscopy. Biophys J. 2008; 94:2819–2831. [PubMed: 17993500]

Eisen JS, Smith JC. Controlling morpholino experiments: don't stop making antisense. Development. 2008; 135:1735–1743. [PubMed: 18403413]

Gao G, Prutzman KC, King ML, Scheswohl DM, DeRose EF, London RE, Schaller MD, Campbell SL. NMR solution structure of the focal adhesion targeting domain of focal adhesion kinase in

complex with a paxillin LD peptide: evidence for a two-site binding model. J Biol Chem. 2004; 279:8441–8451. [PubMed: 14662767]

Geiger B, Bershadsky A, Pankov R, Yamada KM. Transmembrane crosstalk between the extracellular matrix--cytoskeleton crosstalk. Nat Rev Mol Cell Biol. 2001; 2:793–805. [PubMed: 11715046]

Gordon SE, Fluck M, Booth FW. Selected Contribution: Skeletal muscle focal adhesion kinase, paxillin, and serum response factor are loading dependent. J Appl Physiol. 2001; 90:1174–1183. discussion 1165. [PubMed: 11181634]

Guyon JR, Steffen LS, Howell MH, Pusack TJ, Lawrence C, Kunkel LM. Modeling human muscle disease in zebrafish. Biochim Biophys Acta. 2007; 1772:205–215. [PubMed: 16934958]

Hagel M, George EL, Kim A, Tamimi R, Opitz SL, Turner CE, Imamoto A, Thomas SM. The adaptor protein paxillin is essential for normal development in the mouse and is a critical transducer of fibronectin signaling. Mol Cell Biol. 2002; 22:901–915. [PubMed: 11784865]

Hassa PO, Hottiger MO. The diverse biological roles of mammalian PARPS, a small but powerful family of poly-ADP-ribose polymerases. Front Biosci. 2008; 13:3046–3082. [PubMed: 17981777]

Henry CA, McNulty IM, Durst WA, Munchel SE, Amacher SL. Interactions between muscle fibers and segment boundaries in zebrafish. Dev Biol. 2005; 287:346–360. [PubMed: 16225858]

Ilic D, Furuta Y, Kanazawa S, Takeda N, Sobue K, Nakatsuji N, Nomura S, Fujimoto J, Okada M, Yamamoto T. Reduced cell motility and enhanced focal adhesion contact formation in cells from FAK-deficient mice. Nature. 1995; 377:539–544. [PubMed: 7566154]

Jones KS, Alimov AP, Rilo HL, Jandacek RJ, Woollett LA, Penberthy WT. A high throughput live transparent animal bioassay to identify non-toxic small molecules or genes that regulate vertebrate fat metabolism for obesity drug development. Nutr Metab (Lond). 2008; 5:23. [PubMed: 18752667]

Kahn RA. Toward a model for Arf GTPases as regulators of traffic at the Golgi. FEBS Lett. 2009; 583:3872–3879. [PubMed: 19879269]

Kanagawa M, Toda T. The genetic and molecular basis of muscular dystrophy: roles of cell-matrix linkage in the pathogenesis. J Hum Genet. 2006

Keppler BR, Archer TK. Chromatin-modifying enzymes as therapeutic targets--Part 1. Expert Opin Ther Targets. 2008; 12:1301–1312. [PubMed: 18781828]

Khalil A. Morphological analysis of HI features. II. Wavelet-based multifractal formalism. Astrophysical Journal Supplement Series. 2006; 165:512–550.

Kimmel CB, Ballard WW, Kimmel SR, Ullmann B, Schilling TF. Stages of embryonic development of the zebrafish. Dev Dyn. 1995; 203:253–310. [PubMed: 8589427]

Koch-Nolte F, Kernstock S, Mueller-Dieckmann C, Weiss MS, Haag F. Mammalian ADP-ribosyltransferases and ADP-ribosylhydrolases. Front Biosci. 2008; 13:6716–6729. [PubMed: 18508690]

Kwan KM, Fujimoto E, Grabher C, Mangum BD, Hardy ME, Campbell DS, Parant JM, Yost HJ, Kanki JP, Chien CB. The Tol2kit: a multisite gateway-based construction kit for Tol2 transposon transgenesis constructs. Dev Dyn. 2007; 236:3088–3099. [PubMed: 17937395]

Li J, Mayne R, Wu C. A novel muscle-specific beta 1 integrin binding protein (MIBP) that modulates myogenic differentiation. J Cell Biol. 1999; 147:1391–1398. [PubMed: 10613898]

Li J, Rao H, Burkin D, Kaufman SJ, Wu C. The muscle integrin binding protein (MIBP) interacts with alpha7beta1 integrin and regulates cell adhesion and laminin matrix deposition. Dev Biol. 2003; 261:209–219. [PubMed: 12941630]

Lieschke GJ, Currie PD. Animal models of human disease: zebrafish swim into view. Nat Rev Genet. 2007; 8:353–367. [PubMed: 17440532]

Link V, Shevchenko A, Heisenberg CP. Proteomics of early zebrafish embryos. BMC Dev Biol. 2006; 6:1. [PubMed: 16412219]

Lock JG, Wehrle-Haller B, Stromblad S. Cell-matrix adhesion complexes: master control machinery of cell migration. Semin Cancer Biol. 2008; 18:65–76. [PubMed: 18023204]

Lunt SJ, Chaudary N, Hill RP. The tumor microenvironment and metastatic disease. Clin Exp Metastasis. 2009; 26:19–34. [PubMed: 18543068]

Myers KR, Casanova JE. Regulation of actin cytoskeleton dynamics by Arf-family GTPases. Trends Cell Biol. 2008; 18:184–192. [PubMed: 18328709]

Park TJ, Mitchell BJ, Abitua PB, Kintner C, Wallingford JB. Dishevelled controls apical docking and planar polarization of basal bodies in ciliated epithelial cells. Nat Genet. 2008; 40:871–879. [PubMed: 18552847]

Parsons MJ, Campos I, Hirst EM, Stemple DL. Removal of dystroglycan causes severe muscular dystrophy in zebrafish embryos. Development. 2002a; 129:3505–3512. [PubMed: 12091319]

Parsons MJ, Pollard SM, Saude L, Feldman B, Coutinho P, Hirst EM, Stemple DL. Zebrafish mutants identify an essential role for laminins in notochord formation. Development. 2002b; 129:3137–3146. [PubMed: 12070089]

Quach NL, Rando TA. Focal adhesion kinase is essential for costamerogenesis in cultured skeletal muscle cells. Dev Biol. 2006; 293:38–52. [PubMed: 16533505]

Robu ME, Larson JD, Nasevicius A, Beiraghi S, Brenner C, Farber SA, Ekker SC. p53 activation by knockdown technologies. PLoS Genet. 2007; 3:e78. [PubMed: 17530925]

Sabe H, Onodera Y, Mazaki Y, Hashimoto S. ArfGAP family proteins in cell adhesion, migration and tumor invasion. Curr Opin Cell Biol. 2006; 18:558–564. [PubMed: 16904307]

Sadkowski T, Jank M, Zwierzchowski L, Siadkowska E, Oprzadek J, Motyl T. Gene expression profiling in skeletal muscle of Holstein-Friesian bulls with single-nucleotide polymorphism in the myostatin gene 5'-flanking region. J Appl Genet. 2008; 49:237–250. [PubMed: 18670060]

Saporita AJ, Maggi LB Jr, Apicelli AJ, Weber JD. Therapeutic targets in the ARF tumor suppressor pathway. Curr Med Chem. 2007; 14:1815–1827. [PubMed: 17627519]

Schaller MD, Borgman CA, Cobb BS, Vines RR, Reynolds AB, Parsons JT. pp125FAK a structurally distinctive protein-tyrosine kinase associated with focal adhesions. Proc Natl Acad Sci U S A. 1992; 89:5192–5196. [PubMed: 1594631]

Schessl J, Zou Y, Bonnemann CG. Congenital Muscular Dystrophies and the Extracellular Matrix. Semin Pediatr Neurol. 2006; 13:80–89. [PubMed: 17027857]

Scheswohl DM, Harrell JR, Rajfur Z, Gao G, Campbell SL, Schaller MD. Multiple paxillin binding sites regulate FAK function. J Mol Signal. 2008; 3:1. [PubMed: 18171471]

Snow CJ, Goody M, Kelly MW, Oster EC, Jones R, Khalil A, Henry CA. Time-lapse analysis and mathematical characterization elucidate novel mechanisms underlying muscle morphogenesis. PLoS Genet. 2008a; 4:e1000219. [PubMed: 18833302]

Snow CJ, Henry CA. Dynamic formation of microenvironments at the myotendinous junction correlates with muscle fiber morphogenesis in zebrafish. Gene Expr Patterns. 2008

Snow CJ, Peterson MT, Khalil A, Henry CA. Muscle development is disrupted in zebrafish embryos deficient for fibronectin. Dev Dyn. 2008b; 237:2542–2553. [PubMed: 18729220]

Stockwin LH, Vistica DT, Kenney S, Schrump DS, Butcher DO, Raffeld M, Shoemaker RH. Gene expression profiling of alveolar soft-part sarcoma (ASPS). BMC Cancer. 2009; 9:22. [PubMed: 19146682]

Tariq M, Azeem Z, Ali G, Chishti MS, Ahmad W. Mutation in the HPGD gene encoding NAD+ dependent 15-hydroxyprostaglandin dehydrogenase underlies isolated congenital nail clubbing (ICNC). J Med Genet. 2009; 46:14–20. [PubMed: 18805827]

Tempel W, Rabeh WM, Bogan KL, Belenky P, Wojcik M, Seidle HF, Nedyalkova L, Yang T, Sauve AA, Park HW, Brenner C. Nicotinamide riboside kinase structures reveal new pathways to NAD+ PLoS Biol. 2007; 5:e263. [PubMed: 17914902]

Thisse B, Heyer V, Lux A, Alunni V, Degrave A, Seiliez I, Kirchner J, Parkhill JP, Thisse C. Spatial and temporal expression of the zebrafish genome by large-scale in situ hybridization screening. Methods Cell Biol. 2004; 77:505–519. [PubMed: 15602929]

Thomas JW, Cooley MA, Broome JM, Salgia R, Griffin JD, Lombardo CR, Schaller MD. The role of focal adhesion kinase binding in the regulation of tyrosine phosphorylation of paxillin. J Biol Chem. 1999; 274:36684–36692. [PubMed: 10593973]

Tzu J, Marinkovich MP. Bridging structure with function: structural, regulatory, and developmental role of laminins. Int J Biochem Cell Biol. 2008; 40:199–214. [PubMed: 17855154]

Wade R, Bohl J, Vande Pol S. Paxillin null embryonic stem cells are impaired in cell spreading and tyrosine phosphorylation of focal adhesion kinase. Oncogene. 2002; 21:96–107. [PubMed: 11791180]

Waller JC, Dhanoa PK, Schumann U, Mullen RT, Snedden WA. Subcellular and tissue localization of NAD kinases from Arabidopsis: compartmentalization of de novo NADP biosynthesis. Planta. 2010; 231:305–317. [PubMed: 19921251]

Webb DJ, Donais K, Whitmore LA, Thomas SM, Turner CE, Parsons JT, Horwitz AF. FAK-Src signalling through paxillin, ERK and MLCK regulates adhesion disassembly. Nat Cell Biol. 2004; 6:154–161. [PubMed: 14743221]

White ES, Baralle FE, Muro AF. New insights into form and function of fibronectin splice variants. J Pathol. 2008; 216:1–14. [PubMed: 18680111]

Yin C, Kiskowski M, Pouille PA, Farge E, Solnica-Krezel L. Cooperation of polarized cell intercalations drives convergence and extension of presomitic mesoderm during zebrafish gastrulation. J Cell Biol. 2008; 180:221–232. [PubMed: 18195109]

Zhao Z, Gruszczynska-Biegala J, Zolkiewska A. ADP-ribosylation of integrin alpha7 modulates the binding of integrin alpha7beta1 to laminin. Biochem J. 2005; 385:309–317. [PubMed: 15361073]

Zolkiewska A, Moss J. The alpha 7 integrin as a target protein for cell surface mono-ADP-ribosylation in muscle cells. Adv Exp Med Biol. 1997; 419:297–303. [PubMed: 9193669]

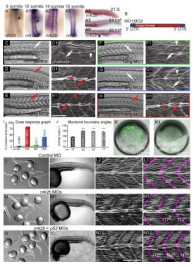

Fig. 1. *nrk2b* expression and MO characterization

(A-A6) ISH with *nrk2b* probe. (A-A3) Dorsal mount, anterior top. (A4-A6) Side mount, anterior left, dorsal top. Black arrowheads denote *nrk2b* expression. (B) Cartoon of *nrk2b* and MO target sites. (C-H1) Side mount, anterior left, dorsal top, 26 hpf embryos, lettered panels are DIC images, numbered panels are phalloidin stained to visualize actin. (C, C1) Injection of a standard control MO did not elicit a phenotype. Myotomes are V-shaped (white arrows) and muscle fibers are normal (white arrowheads). Injection of the functional dose of MO1 (D, D1) or MO2 (E, E1) resulted in U-shaped myotomes (red arrows) and wavy muscle fibers (red arrowheads). Injection of half the functional dose of MO1 (F, F1) or MO2 (G, G1) did not disrupt muscle development. (H, H1) Injection of both low doses of MO1 + MO2 recapitulated the phenotype. (I) Dose response graph. Injection of low doses of MO1 + MO2 resulted in more embryos with the phenotype than injection of either low dose alone (n of embryos injected is listed on the x-axis). (J) Average myotome boundary angles of 26 hpf control, *laminin γ 1* mutants, *nrk2b* morphant, and *nrk2b* + *p53* MO-injected embryos. *laminin γ1* mutants, *nrk2b* morphants, and *nrk2b* + *p53* morphants have myotome boundaries of a similar angle and all have myotome boundary angles that are significantly wider than controls, $p<0.001$ (n of MTJs measured is listed on the x-axis). (K-K1) Brightfield images of shield stage embryos. Animal pole to the top. (K) Embryo injected with the *nrk2b:gfp* plasmid that contains both MO target sites. (K1) Embryo injected with the *nrk2b:gfp* plasmid and *nrk2b* MOs. Note that expression of GFP-tagged Nrk2b is drastically decreased by injection of *nrk2b* MOs (3 experiments, 1 representative experiment: 93% of *nrk2b:gfp* injected embryos expressed GFP (n=171 out of 184 embryos) whereas only 5% of *nrk2b:gfp* + *nrk2b* MO injected embryos expressed any GFP (n=1 out of 20 embryos)). (L-N) Brightfield images of a dish of 26 hpf embryos. (L-L1) Control MO-injected embryos. (M-M1) *nrk2b* morphants. (N-N1) *nrk2b* + *p53* morphants. (L1-N1) Side mount, anterior left, dorsal top, 26 hpf embryos, DIC imaging. Higher magnification images of one representative embryo from each of the corresponding dishes. Note that the control morphant (L1) has a longer body axis than both *nrk2b* morphants (M1) and *nrk2b* + *p53* double morphants (N1). (L2-N3) Side mount, anterior left, dorsal top, 26 hpf embryos, phalloidin staining to visualize actin. Higher magnification views of embryos from the corresponding dishes. In panels numbered 3, myotome boundaries were pseudocolored fuschia and the myotome boundary angle is given with the corresponding boundary. Note that while injection of *p53* MO did rescue the cell death seen in the head of *nrk2b* morphants, it did not rescue the shorter body axis (compare M1 to N1) or the U-shaped myotomes (compare M3 to N3). Scale bars are 50 μm, *** $p< 0.001$.

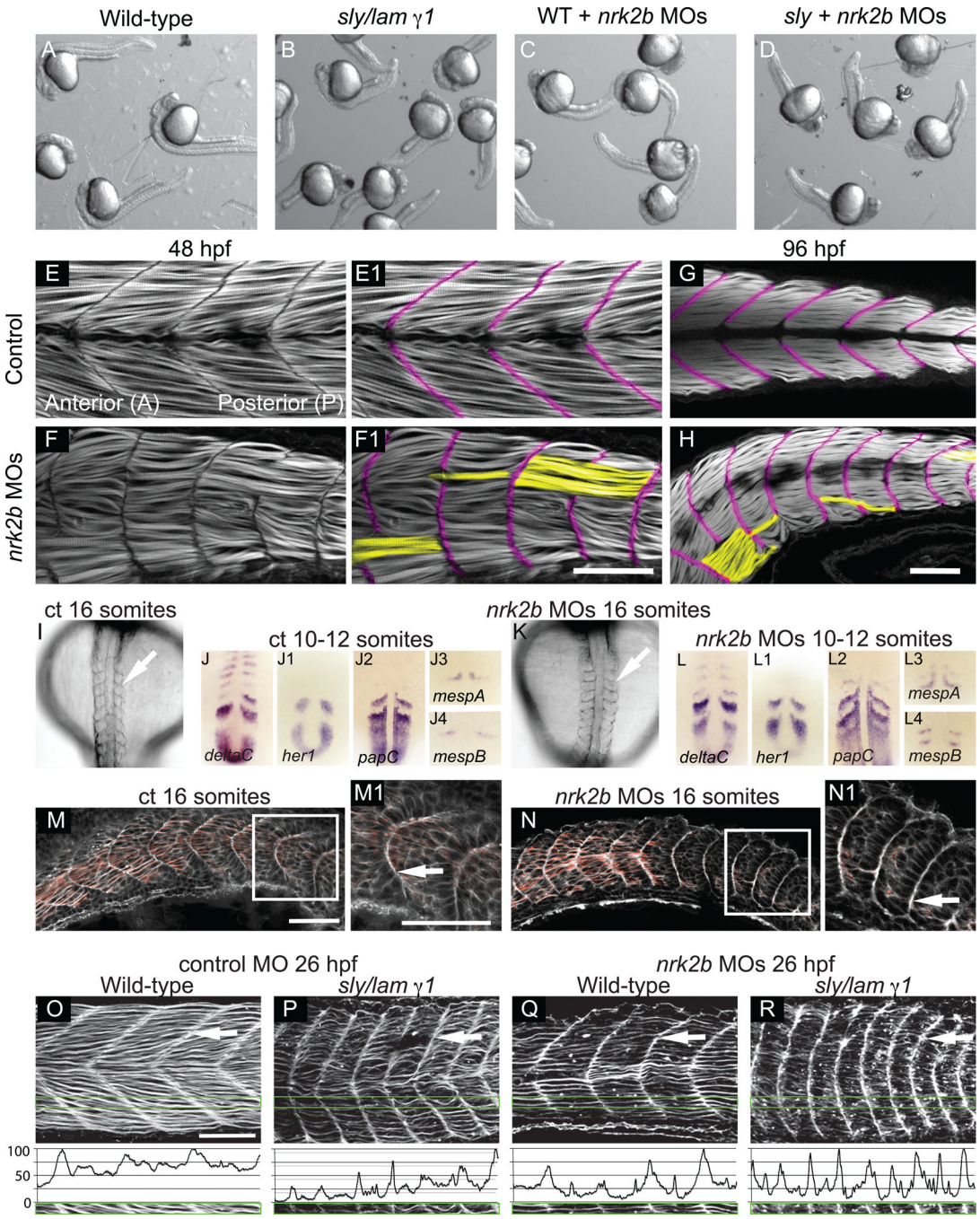

Fig. 2. Disrupted MTJs in *nrk2b* morphants are not due to discontinuous initial somite boundaries

(A-D) Brightfield images of a dish of 26 hpf embryos. (A) Wild-types. (B) *sly/laminin γ1* mutants. (C) *nrk2b* morphants. (D) *nrk2b* MO in*jected-laminin γ1* mutants. Note that injection of *nrk2b* MOs into *laminin* mutants does not drastically worsen their phenotype or result in death. (E-H) Side mount, anterior left, dorsal top, phalloidin stained embryos, MTJ boundaries are pseudocolored fuschia and abnormally long muscle fibers are pseudocolored yellow. (E-E1) 48 hpf control. (F-F1) 48 hpf *nrk2b* morphant (71/212, 33% of MTJs are crossed by muscle fibers). (G) 96 hpf control. (H) 96 hpf *nrk2b* morphant (19/67, 28% of MTJs are crossed by muscle fibers). (I, K) Dorsal mount, anterior top, 16 S, brightfield

images. Note that somite boundaries form (white arrows) in *nrk2b* morphants (K). (panels J, L) Dorsal mount, anterior top, 10–12 S, ISH for known somite patterning and somite boundary formation genes. Note that the domains and patterns of expression are similar between controls (panels J) and *nrk2b* morphants (panels L). (M-N) Side mount, anterior left, dorsal top, 16 S, phalloidin staining. Note concentrated actin at the initial somite boundary (white arrows). These data show that discontinuous MTJs are not due to discontinuous initial somite boundaries. (O-R) Side view, anterior left, dorsal top, 26 hpf embryos, phalloidin stained to visualize actin. (O-P) Control MO-injected. (Q-R) *nrk2b* MO-injected. (O, Q) Wild-types. (P, R) *sly/laminin γ1* mutants. Note that in *laminin* mutants and *nrk2b* morphants, actin is enriched at the MTJ (white arrows) and lacking in the myotome. Green boxes correspond to normalized fluorescence intensity (see methods) plots. These graphs support the qualitative actin disruption seen in *laminin* mutants and *nrk2b* morphants. Scale bars are 50 μm.

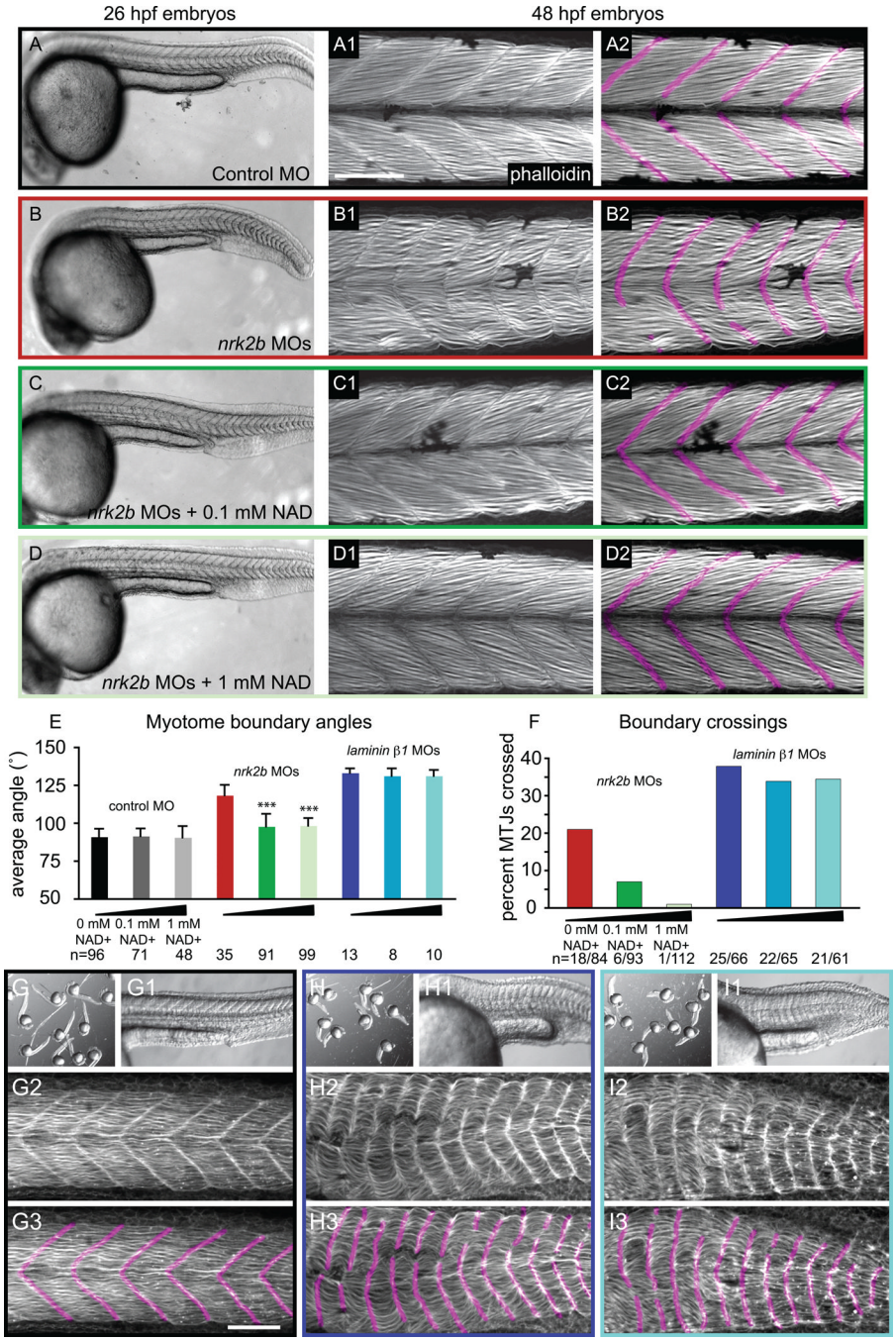

Fig. 3. Exogenous NAD+ treatment rescues the *nrk2b* morphant muscle phenotype

(A-D) Brightfield images, side mount, anterior left, dorsal top, 26 hpf embryos. (numbered panels A-D) Side mount, anterior left, dorsal top, 48 hpf embryos, phalloidin stained to visualize actin. In panels numbered 2, MTJs are pseudocolored fuschia. (panels A) Control MO-injected. (panels B) *nrk2b* MO-injected. (panels C) *nrk2b* MO-injected embryos incubated in 0.1 mM NAD+. (panels D) *nrk2b* MO-injected embryos incubated in 1 mM NAD+. (E) Graph of average myotome boundary angles in controls, NAD+-treated controls, *nrk2b* morphants, NAD+-treated *nrk2b* morphants, *laminin* morphants, and NAD+-treated *laminin* morphants. The average myotome boundary angle of *nrk2b* morphants is significantly different than controls (student t-test, $p < 0.001$) and the average myotome

boundary angle of NAD+-treated *nrk2b* morphants is significantly different than untreated *nrk2b* morphants and controls (student t-test, $p < 0.001$, n of myotome boundaries measured on x-axis). (F) Graph of the percent of MTJs crossed by muscle fibers in *nrk2b* morphants, NAD+-treated *nrk2b* morphants, *laminin* morphants, and NAD+-treated *laminin* morphants. NAD+ treatment rescues boundary crossings in a dose dependent manner in *nrk2b* morphants, but not *laminin* morphants (n of MTJs crossed over total MTJs analyzed is listed on the x-axis). (panels G) Controls. (panels H) *laminin* morphants. (panels I) 1mM NAD+-treated *laminin* morphants. (lettered panels) Brightfield images of a dish of embryos. (panels numbered 1) Side mount, brightfield images, 26 hpf embryos, anterior left, dorsal top. (panels numbered 2) Side mount, 48 hpf embryos, anterior left, dorsal top, phalloidin stained to visualize actin. (panels numbered 3) MTJs are pseudocolored fuschia. Scale bars are 50 μm, *** $p < 0.001$.

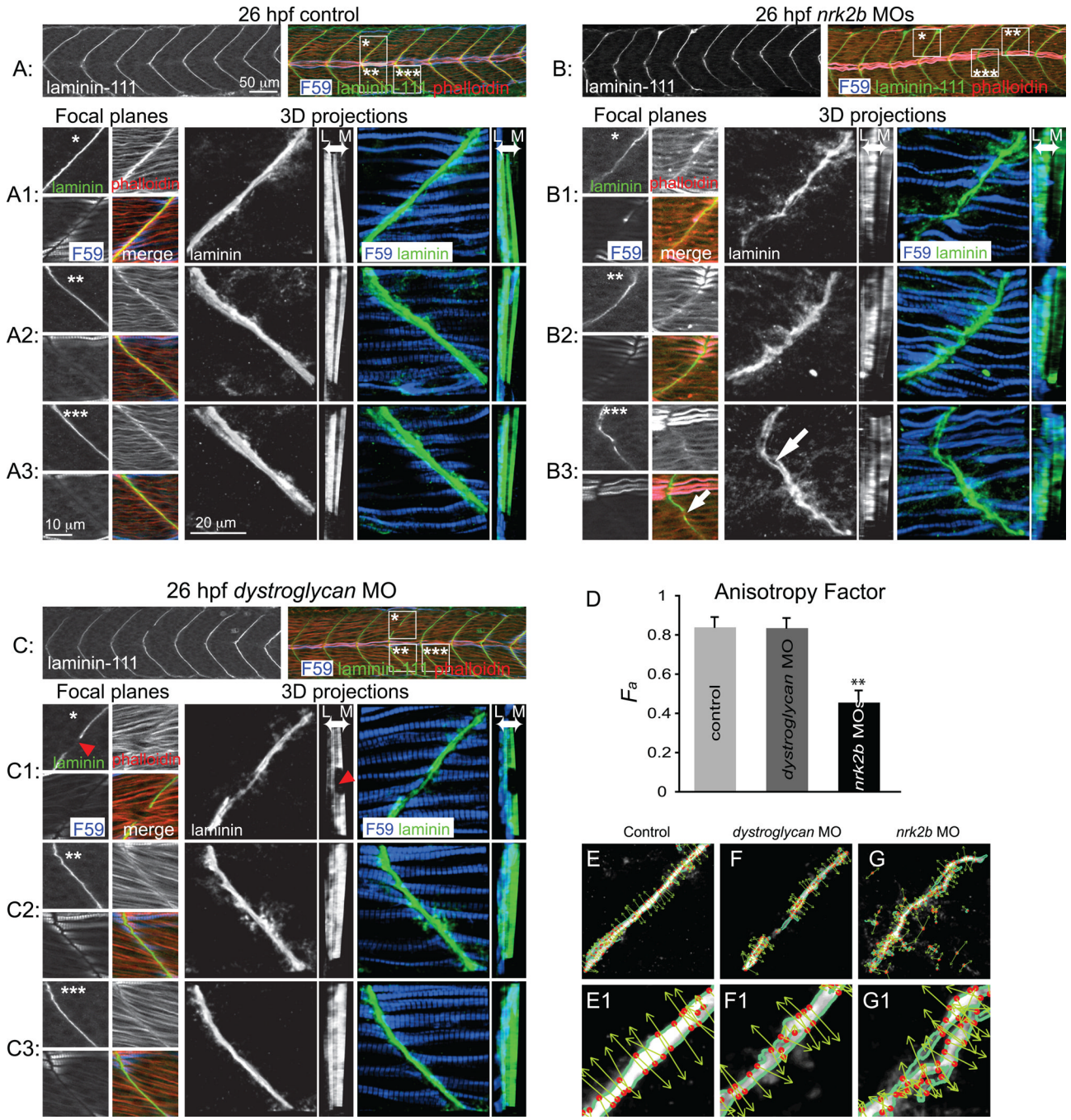

Fig. 4. Nrk2b is required for normal basement membrane development

(A, B, C) 26 hpf embryos, side mount, anterior left, dorsal top, F59 antibody stained to visualize slow-twitch muscle, phalloidin stained to visualize actin and Laminin-111 antibody stained to visualize the basement membrane of the MTJ. Also see supplemental movies. (A) Control. (B) *nrk2b* morphant. (C) *dystroglycan* morphant. Numbered panels 1–3 are examples of different MTJs within an embryo from each treatment (*, ** or *** indicates the location of the MTJ). Small square panels are focal planes of each antibody/stain used as well as a merged view. Large square panels are 3D reconstructed Laminin-111 antibody staining (in black and white) or F59 and Laminin-111 antibody staining (in color). Tall rectangular panels are transverse views of the 3D reconstructed antibody staining with

lateral to the left and medial to the right. Note in the MTJ examples in *nrk2b* morphants (panels B) that Laminin-111 is not laid down in a straight line and is not always continuous (white arrows). In the transverse views, note that Laminin-111 is especially disrupted in the medial fast-twitch fiber domain. In *dystroglycan* morphants, MTJs can still be discontinuous (red arrowheads), but Laminin-111 is robust in the lateral and medial domains. (D) Graph of the anisotrophy factor (see methods) in Laminin-111 stained images. A lower anisotrophy value in *nrk2b* morphant images indicates that there is less order/structure in Laminin-111 staining in these morphants. (E-G) Side mount, anterior left, dorsal top, 26 hpf embryos, Laminin-111 antibody staining. Numbered panels are higher magnification views of corresponding panels. Images were analyzed with the 2D Wavelet Transform Modulus Maxima (2DWTMM) method. (panels E) Controls. (panels F) *dystroglycan* morphants. (panels G) *nrk2b* morphants. In controls and *dystroglycan* morphants, the vectors are more parallel indicating more order than in *nrk2b* morphants. Scale bars are labeled on the figure, ** $p<0.01$.

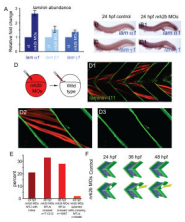

Fig. 5. Nrk2b is non-cell autonomously required for normal basement membrane polymerization

(A) qRT-PCR for relative transcript abundance of the three *laminin* chains that comprise Laminin-111 in 24 hpf embryos. (B-C) Side mount, anterior left, dorsal top, 24 hpf. ISH for *laminin* transcripts in controls (lettered panels) and *nrk2b* morphants (numbered panels), (panels B) *laminin α1*, (panels C) *laminin γ1*. ISH and qRT-PCR suggest that Laminin-111 defects in *nrk2b* morphants are not due to a *laminin* transcription deficiency. (D) Model of dextran labeled *nrk2b* morphant cells being transplanted into a wild-type host at blastula stage. (D1-D3) Side mount, anterior left, dorsal top, 48 hpf, red cells are dextran labeled Nrk2b-deficient cells. Laminin-111 antibody staining (in green) is normal adjacent to Nrk2b-deficient cells (red) in a wild type background. This suggests that basement membrane polymerization is a phenomenon mediated by communities of cells and that Nrk2b is non-cell autonomously required for basement membrane polymerization. (E) Graph of the percentage of MTJs with holes in Laminin-111 or with boundary crossings over time. The observation that the percentage of MTJs with defects does not steadily increase over time suggests that boundary crossings are not due to age-dependent degeneration of the MTJ. Note that a very small percentage of Nrk2b-deficient cells cross MTJs in wild-type hosts suggesting that these cells do not actively degrade Laminin-111 and that Nrk2b functions non-cell autonomously in basement membrane development. (F) Model of MTJ basement membrane defects in *nrk2b* morphants leading to fibers crossing MTJs as time progresses.

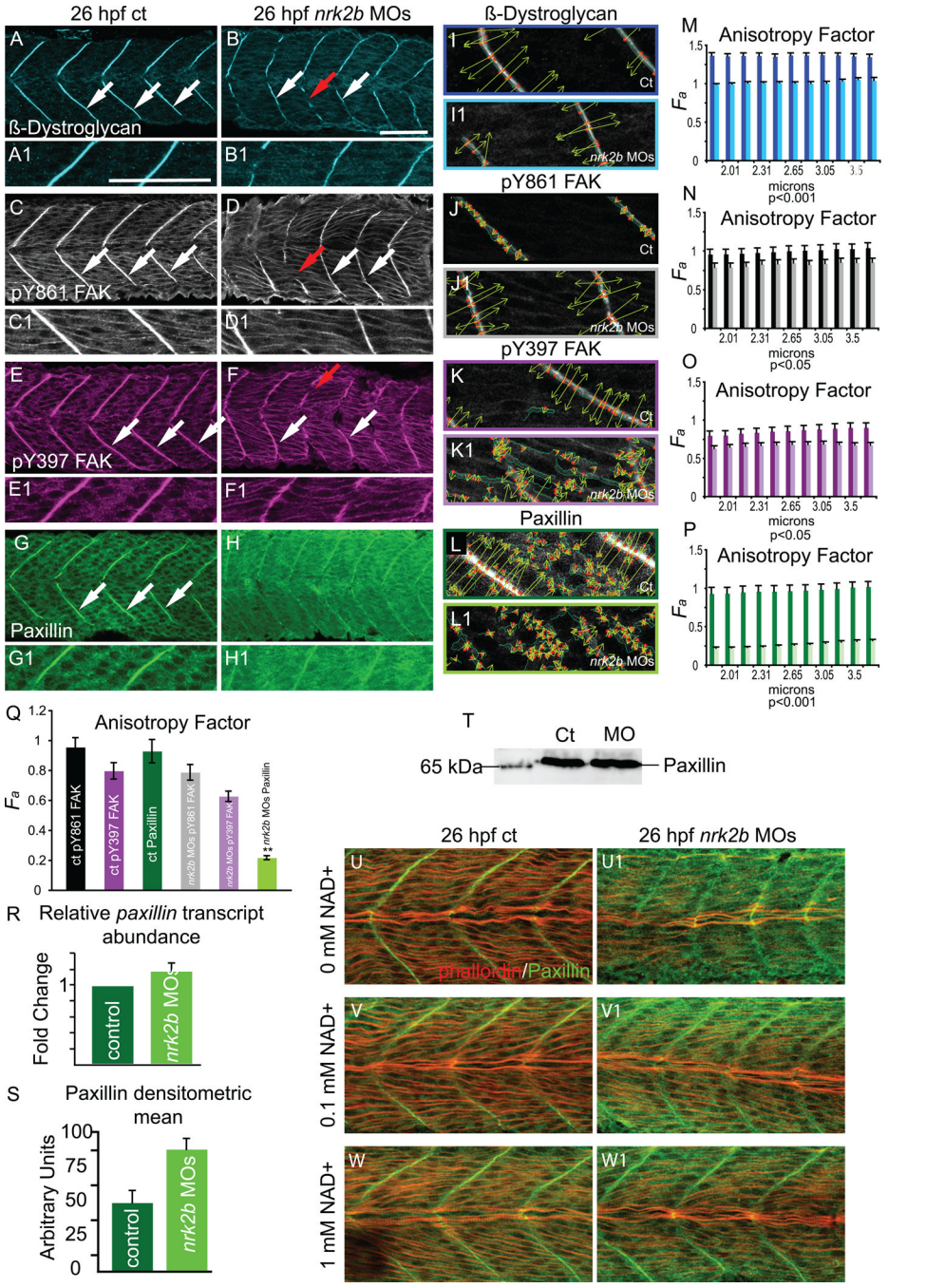

Fig. 6. Nrk2b is required for normal subcellular localization of Paxillin, but not *β*-Dystroglycan or FAK

(A-H) Side mount, anterior left, dorsal top, 26 hpf. Panels A, C, E, and G are controls. Panels B, D, F, and H are *nrk2b* morphants. Panels numbered 1 are magnifications of the corresponding lettered panels. (A-B1) *β*-Dystroglycan antibody staining. (C-D1) pY861 FAK antibody staining. (E-F1) pY397 FAK antibody staining. (G-H1) Paxillin antibody staining. White arrows indicate normal localization of proteins to MTJs. Red arrows in *nrk2b* morphants (B, D, F) indicate discontinuous MTJs crossed by muscle fibers. Note that in *nrk2b* morphants (H, H1), Paxillin does not robustly concentrate to MTJs. (I-L) Side mount, anterior left, dorsal top, 26 hpf controls (lettered panels) and *nrk2b* morphants

(numbered panels). Application of 2D WTMM method showing maxima chains (dark green), nodes (red), and vectors (light green) for CMAC component antibody staining. (M-Q) Graphs of anisotropy or the amount of order in a structure over a range of applicable size scales. (R) qRT-PCR, (S) average densitometric mean of Paxillin antibody-stained images and (T) Western analysis suggest that Paxillin levels are not decreased in *nrk2b* morphants. (U-W) Side mount, anterior left, dorsal top, 26 hpf embryos, phalloidin staining in red, Paxillin antibody staining in green. Lettered panels are controls and numbered panels are *nrk2b* morphants. (panels U) No exogenous NAD+. (panels V) 0.1 mM exogenous NAD+. (panels W) 1 mM exogenous NAD+. Note that exogenous NAD+ treatment rescues medial Paxillin concentration at the MTJ in *nrk2b* morphants in a dose dependent manner. Scale bars are 50 μm.

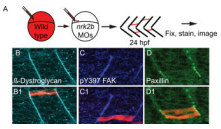

Fig. 7. Nrk2b is cell-autonomously required for Paxillin localization to MTJs

(A) Cartoon showing dextran labeled wild-type cells being transplanted into a *nrk2b* morphant host at blastula stage. (B-D) Side mount, anterior left, 26 hpf *nrk2b* morphant hosts with transplanted wild-type cells (red), *β*-Dystroglycan antibody staining (light blue, panels B), pY397 FAK antibody staining (dark blue, panels C), and Paxillin antibody staining (green, panels D). Note that *β*-Dystroglycan and pY397 FAK robustly localize to MTJs in *nrk2b* morphants in the presence and the absence of transplanted wild-type cells. Note that robust Paxillin localization to the MTJ in *nrk2b* morphants is rescued in the transplanted wild-type cells, but not in the Nrk2b-deficient cells surrounding them.

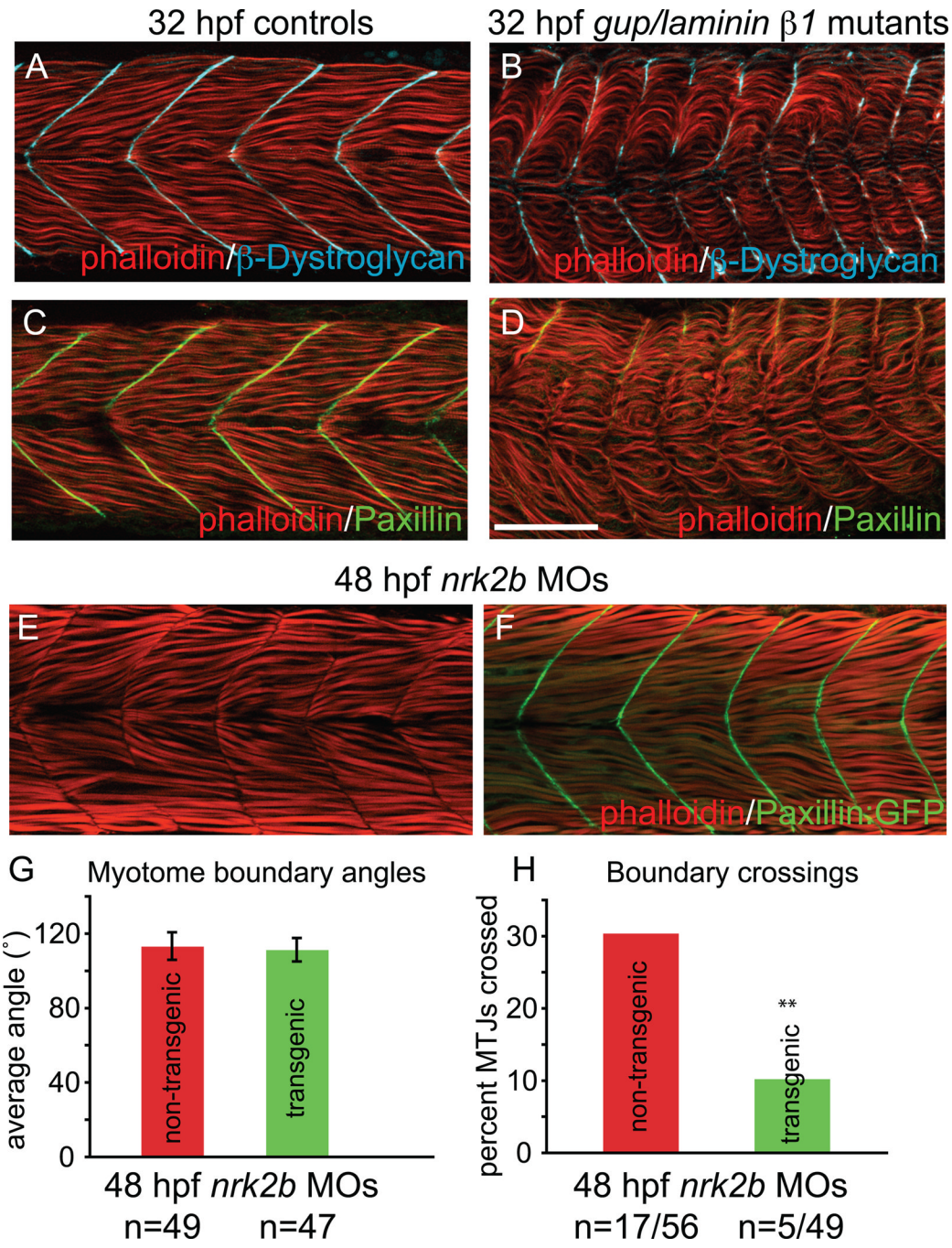

Fig. 8. Paxillin overexpression rescues MTJ integrity in *nrk2b* morphants

(A-D) Side mount, anterior left, dorsal top, 32 hpf controls (panels A and C) *gup/laminin β1* mutants (panels B and D) stained with phalloidin (red), β-Dystroglycan (blue) and Paxillin (green). Note that the Paxillin is severely disrupted in *gup/laminin β1* mutants, suggesting that adhesion to Laminin plays a role in Paxillin localization. (E-F) Side mount, anterior left, dorsal top, 48 hpf embryos. (E) *nrk2b* morphant. Note that approximately 1/3 of MTJs are crossed by muscle fibers. (F) *nrk2b-MO* injected Paxillin:GFP transgenic zebrafish. Note that overexpression of Paxillin:GFP greatly reduces the frequency of boundary crossings in *nrk2b* morphants. (G) Graph of myotome boundary angles. Note that overexpression of Paxillin:GFP does not rescue the wider myotome boundary angles observed in *nrk2b*

morphants (n of myotome boundary angles measured is on the x-axis). (H) Graph of percentage of MTJs crossed by muscle fibers. Note that overexpression of Paxillin:GFP does significantly rescue boundary crossings in *nrk2b* morphants (n of crossed MTJs over total MTJs analyzed is on the x-axis). Scale bar is 50 μm, ** $p<0.01$.

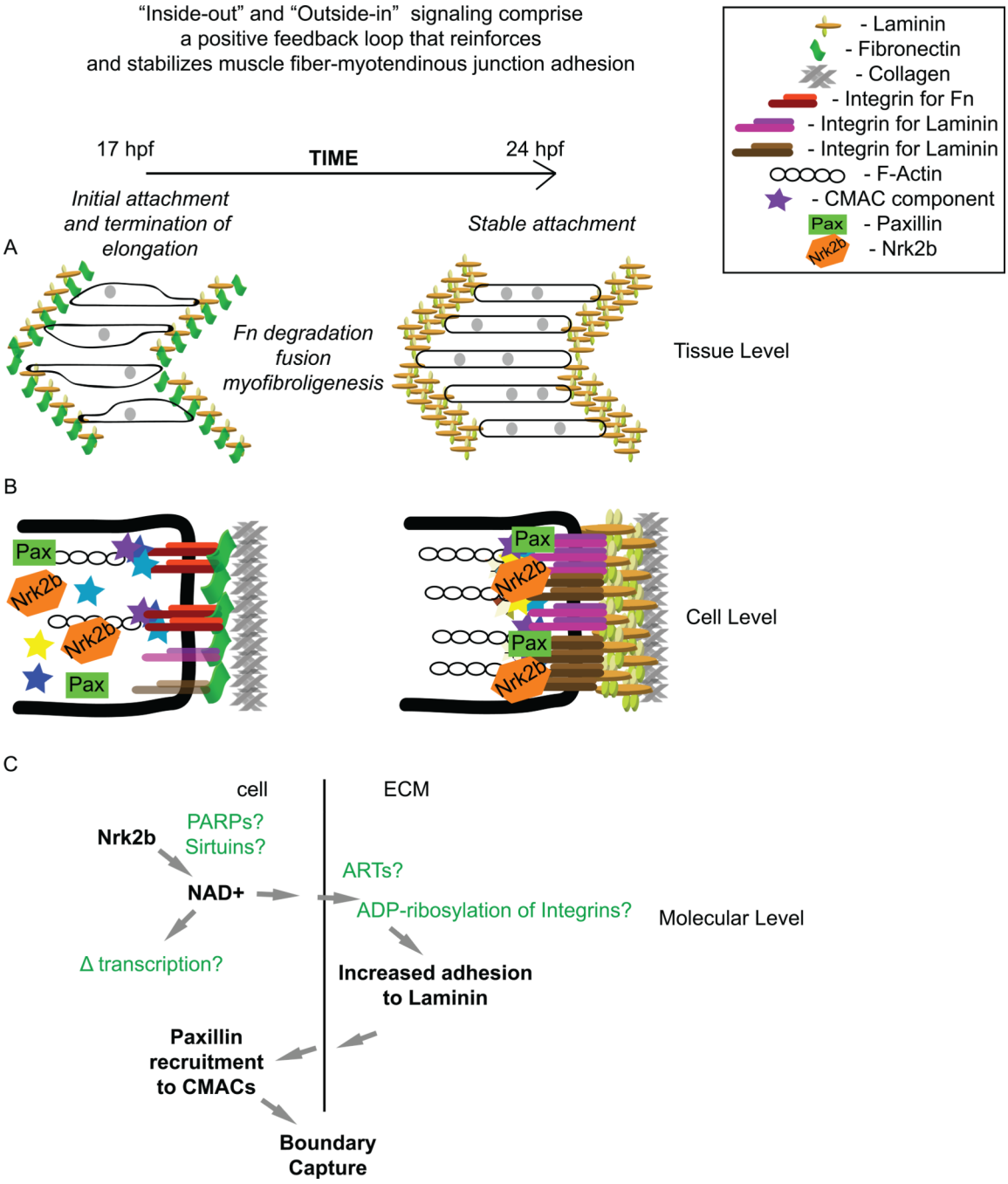

Fig. 9. Roles for cell-matrix adhesion during muscle morphogenesis

(A) Cartoon of steps involved in muscle morphogenesis between 17 hpf and 24 hpf at the tissue level. During this time, myotube shape becomes more regular, fusion occurs, Fn is degraded, and Laminin polymerization increases. (B) Cartoon of CMAC formation and the modulation of the specificity of CMACs between 17 hpf and 24 hpf. Note the increase in cell-matrix adhesion complex formation. (C) Cartoon of molecular level events during muscle morphogenesis involving Nrk2b and NAD+. The main molecular function of Nrk2b is to produce NAD+ via an alternative salvage pathway. NAD+ is an obligatory substrate for enzymes such as poly-ADP-ribose polymerases (PARPs), and Sirtuins. Ecto-mono-ADP-ribosyltransferases (ARTs) are hypothesized to ADP-ribosylate Integrins, increasing their

binding affinity for Laminin in an irreversible reaction. NAD+ is also believed to modulate gene transcription via regulation of Sirtuin activity. Increased adhesion to Laminin can promote Paxillin recruitment to CMACs. Paxillin, in turn, mediates boundary capture and termination of muscle cell elongation.